Adverse Rotorcraft-Pilot Couplings - Modelling and Prediction of Rigid Body RPC. Sketches from the Work of European Project ARISTOTEL 2010-2013

M.D. Pavel, D. Yilmaz, B. Dang Vu, M. Jump, L. Lu, M. Jones

HAL Id: hal-01061152

https://onera.hal.science/hal-01061152

Submitted on 5 Sep 2014

Adverse Rotorcraft-Pilot Couplings – Modelling and Prediction of Rigid Body RPC *Sketches from the Work of European Project ARISTOTEL 2010-2013*

Marilena D. Pavel
Deniz Yilmaz
Delft University of Technology
Kluyverweg 1
NL-2629 HS Delft
The Netherlands
Tel.: +31 15 278 39 92
Fax.: +31 15 278 34 44
m.d.pavel@tudelft.nl
d.yilmaz@tudelft.nl

Binh Dang Vu
ONERA
Base Aerienne 701
FR-13661 Salon de Provence
France
Tel.: +33 4 90 17 01 02
Fax.: +33 4 90 17 01 09
binh.dangvu@onera.fr

Michael Jump
Linghai Lu
Michael Jones
University of Liverpool
Room 2.05 Chadwick Tower Peach Street
Liverpool L69 7ZF
UK
Tel.: +44 151 794 6845
Fax.: +44 151 794 6841
mjump1@liverpool.ac.uk
linghai}@liverpool.ac.uk
michael.jones@liverpool.ac.uk

Abstract

Unfavourable Aircraft/Rotorcraft Pilot Couplings (A/RPCs), usually called pilot induced oscillations (PIO), manifested themselves since the early days of manned flight and may still create problems in modern configurations. In Europe, the ARISTOTEL project (Aircraft and Rotorcraft Pilot Couplings – Tools and Techniques for Alleviation and Detection) was set up with the aim of understanding and improving the available tools used to unmask A/RPCs. The goal of the present paper is to give an overview of the work performed on rotorcraft rigid body RPC. Rigid body RPC involve adverse coupling phenomena dominated by helicopter lower frequency dynamics with pilot in the loop. Using as example the Bo-105 helicopter enhanced by a rate command attitude hold control system, the paper will demonstrate the applicability of bandwidth-phase delay and OLOP criteria to unmask Cat I PIO and respectively Cat II PIO. The paper will introduce a novel on-line prediction algorithm, the so- called PRE-PAC (phase aggression criterion) based on analysis of the phase distortion between the pilot input and vehicle response. Special attention will be given to pilot modelling for RPC detection in the so-called boundary avoidance tracking (BAT) concept. In this sense, the paper will determine the critical boundary size leading to a RPC in a tracking task and will connect this to the optical tau theory. Bifurcation theory will be applied to a BAT pilot-vehicle system in a roll step manoeuvre mainly for prediction of Cat III PIO.

NOMENCLATURE

APC	Aircraft Pilot Coupling
BAT	Boundary Avoidance Tracking
BPD	Bandwidth Phase Delay
FCS	Flight Control System
HQ	Handling Qualities
OLOP	Open Loop Onset Point
PAC	Phase-Aggression Criterion
PIO	Pilot Induced Oscillation
PIOR	PIO Rating
PST	Peak Selection Threshold
PT	Point Tracking
PVS	Pilot Vehicle System
RC	Rate Command
ROVER	Real-time Oscillation Verifier
RPC	Rotorcraft Pilot Coupling

1. INTRODUCTION AND BACKGROUND

During the development and operation of aircraft and rotorcraft, it appears that both, engineers and pilots, must be prepared to deal with unfavourable phenomena, the so-called "Aircraft/Rotorcraft Pilot Couplings" (A/RPCs).

Generally, A/RPCs are adverse, unwanted phenomena originating from anomalous and undesirable couplings between the pilot and the aircraft/rotorcraft. These undesirable couplings may result in annoying oscillatory/non-oscillatory instabilities which degrade the flying qualities, increase the structural strength requirements and sometimes can result in catastrophic accidents. The understanding of the occasional and yet dramatic appearances of

A/RPCs has driven significant past research, which continues in the present and will no doubt present challenges for the future. A/RPCs can be extraordinary and memorable events involving unique, fascinating and often apparently unpredictable complex dynamic interactions between the pilot and the air vehicle.

The understanding of the occasional and yet dramatic appearances of A/RPCs has driven significant past research, which continues in the present and will no doubt present challenges for the future. The reason for this is that A/RPCs usually are extraordinary and memorable events involving unique, fascinating and often apparently unpredictable complex dynamic interactions between the pilot and the air vehicle. From the early days of Wright Brothers flights [1] when aircraft were toppling over during operations in gusty conditions to modern fly-by-wire aircraft, A/RPCs existed and the problem of eliminating such phenomena is not yet solved. In 2010 the European Commission launched, under the umbrella of the 7th Framework Programme (FP7), the ARISTOTEL project (Aircraft and Rotorcraft Pilot Couplings – Tools and Techniques for Alleviation and Detection), the aim of which is to advance the state-of-the-art of A/RPC prediction and suppression. With a duration of 3 years, starting from October 2010, and involving partners from across Europe [2, 3], the ARISTOTEL project's objectives were to improve the physical understanding of present and future A/RPCs and to define criteria to quantify an aircraft's susceptibility to A/RPC. The present paper is a synthesis of the work performed on rigid body modelling and prediction of rotorcraft pilot couplings (RPC).

Rigid body RPC are also known in the specialists' community as Pilot induced Oscillations (PIO) as they were named like this until 1995. Rigid body RPC (PIO) generally occur when the pilot inadvertently excites divergent vehicle oscillations by applying control inputs that are in the wrong direction or have phase lag with aircraft motion. Since the active involvement of the pilot in the control loop is pre-requisite, the oscillations will cease when the pilot releases the controls, stops providing control inputs or changes the control strategy. Of course, for this to happen, the pilot must recognise that a PIO is in progress and must be in a position to be able to take corrective action.

Next to the class of rigid body RPC/ PIO problems one can encounter the class of Aeroelastic RPC or pilot Assisted Oscillations (PAO). PAO are the result of involuntary control inputs by the pilot in the loop that may destabilize the aircraft due to inadvertent man-machine couplings. Generally, for a PAO to occur, involuntary involvement of the pilot due to his biodynamic response to vibrations is required. The present paper will concern only the area of rigid body RPC/ PIO, leaving the area of PAO for a separate analysis.

There are a few typical characteristics for A/RPCs that distinguish from other dynamic instabilities:

- A/RPCs always involve a "collaborative effort" between the pilot and the vehicle in the so-called "pilot-vehicle system" (PVS). Without the pilot, A/RPC cannot occur and pilot's voluntary or involuntary actions depend to some degree, on the vehicle motion and characteristics.

- A/RPCs are associated with three crucial ingredients: 1) an abnormal/unexpected change in pilot behaviour 2) an abnormal/unexpected change in the vehicle dynamics state or configurations and 3) an initiation mechanism commonly referred to as a 'trigger'. Each of these factors, in and of themselves, cannot create an A/RPC, but given the right circumstances, the pilot, through active or passive participation can interact with the rigid body airframe motion or with the low frequency airframe structural modes, frequently via flight control system (FCS) interaction, to induce an A/RPC instability.

- Typically, during an adverse A/RPC event, the pilot switches his/her strategy from using small, gentle control inputs to overcorrecting with large inputs even for small errors. The result is often an out-of-phase condition, which results in pilot-induced changes in vehicle attitude.

- A/RPCs are very often explosive in nature; the instability of the PVS develops in a few seconds to levels uncontrollable for the pilot.

Table 1 summarizes the characteristics of rigid body and aeroelastic RPCs as described in the ARISTOTEL project. One can see that rigid body RPC belong to the low frequency range RPC at frequencies of approximately 1.5 Hz and below. They are dominated, by helicopter low frequency dynamics i.e. flight mechanics characteristics, by the flight control system and by an active pilot "keen" to fulfil the mission task properly by actively controlling the aircraft. The ARISTOTEL group believed that for rotorcraft one can define a group of

"Extended" rigid body RPC related to the extension of a classical 6-degree of freedom body modelling to the low-frequency modes of the rotor dynamics, the control actuators dynamics, the SAS dynamics effects or the digital system time delays. This class of RPCs can be seen as the blending area between rigid body and aeroelastic RPCs and will need special tools and methods for analysis.

Table 1 Characterisation of 'Rigid Body' and 'Extended' Rigid body RPC

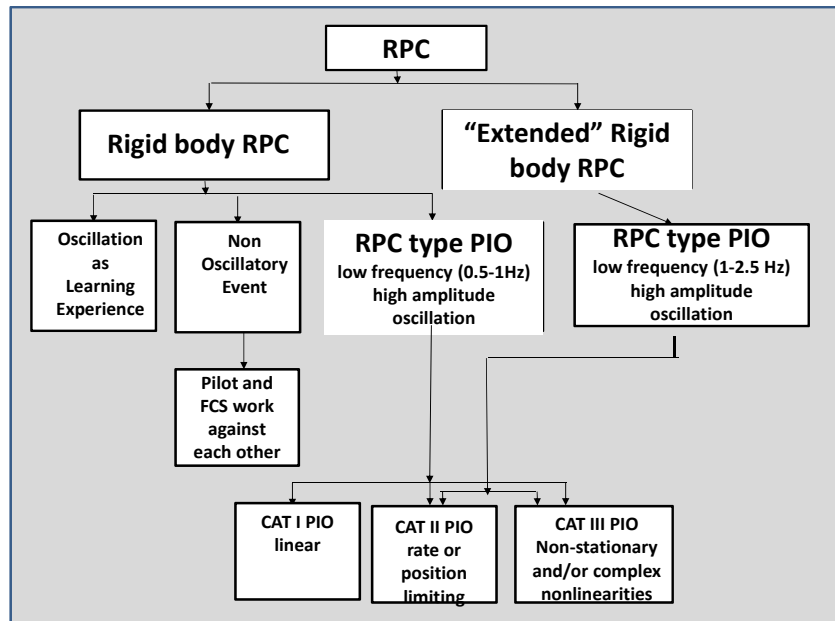|	Low frequency A/RPCs	High frequency A/RPCs	
	Rigid body aircraft dynamics	**Extended Rigid body aircraft dynamics**	**Elastic body aircraft**
Frequencies	**Below 1.5 Hz** *APC frequencies are usually within 0.5-1.6 Hz (3-10 rad/sec).*	**Between 1.5-2 Hz (APC)** **Below 3.5 Hz (RPC)** *APCs frequencies usually exceed 2 Hz. Examples: Roll Ratchet, bob-weight.*	**Between 2-8 Hz**
Causes	1) Inadequate vehicle dynamic characteristics (aircraft + control system): • High order of the system, large phase delay, low damping, and others. • Control system delay. • Actuator or control surface rate limit. 2) High control sensitivity (command gain), low force-displacement gradient.	1) Biodynamic interaction: The biodynamic interaction in the "pilot + manipulator + aircraft" system arises due to high-frequency aircraft response to pilot activity caused by inadequate aircraft characteristics (high natural frequencies, low roll mode time constant, high control sensitivity, large pilot location relative to the centre of gravity)	1) Biodynamic interaction: The biodynamic interaction in the pilot-aircraft system arises due to aircraft structural elasticity and leads to involuntary manipulator deflections transferred to control system.
Characteristics	Pilot closes the loop according to the information received through visual or acceleration perception channels.	The pilot closes the control loop due to **aircraft accelerations** acting on the body and the arm cause involuntary manipulator deflections which go to the control system and lead to high-frequency A/RPC.	The pilot closes the control loop due to **structural oscillations and inertial forces** acting on the body and the arm cause involuntary manipulator deflections which go to the control system and provoke high-frequency A/RPC.
Critical components		Flight control system	Airframe modes
Pilot modelling	'Active' pilot concentrating on a task	'Active' pilot concentrating on a task	'Passive' pilot subjected to vibrations
Vehicle dynamics modelling	Flight mechanics	Flight mechanics	Structural dynamics

Figure 1 Classification of rigid body RPC's [based on 4])

The project considered also the classical McRuer et. al. [4] division of RPCs according to the degree of non-linearity of the pilot vehicle system (PVS) (see Figure 1). RPC as a learning experience is the simplest form of pilot-vehicle oscillations and can happen on any aircraft. "*Inappropriate behavioural organization and adaptation as well as an excessive pilot gain are common in early flight operations with new aircraft. The oscillations are associated with the pilot's inexperience and may disappear as the pilot adapts a more appropriate system organization and/or transfer characteristic.*" [4] Non-oscillatory RPC events involve PVS motions that, although not oscillatory, still derive from inadvertent pilot-vehicle interactions. Although no non-oscillatory RPC has been mentioned in the literature for rotorcraft, for fixed-wing aircraft, such events are a consequence of the implementation of auxiliary functions into the AFCS such as wind gusts alleviation, loads control during aircraft manoeuvres and automatic control of the aircraft operating points. (a famous non-oscillatory APC event was encountered in the development of the SAAB JAS-39 Gripen during a public demonstration in 1993). The most usual subdivision of rigid body A/RPCs is related to Category I PIO essentially linear PVS oscillations; Category II PIO quasi-linear PVS oscillations; Category III PIO essentially nonlinear PVS oscillations. The paper will follow this categorisation in describing the criteria existing for RPC prediction.

The paper is structured as follows: after a short Introduction and description of rigid body RPCs, Chapter 2 will concentrate on vehicle modelling. Chapter 3 discusses mainly pilot modelling for rigid body RPCs, describing on the one hand the classical cross-over pilot model and on the other hand new pilot models obtained through identification techniques or boundary avoidance tracking. Traditional and new RPC prediction tools are applied theoretically and then verified experimentally during simulator sessions in Chapter 4. General conclusions on the rigid body RPC problem are given in Chapter 5.

2. HELICOPTER MODELLING FOR RIGID BODY RPC

As discussed in the Introduction, one of the three crucial A/RPC ingredients is the unfavourable vehicle dynamics. This means that the vehicle system as a whole, including the FCS, displays, actuators, etc., should be prone to A/RPC. The occurrence of A/RPC is regarded by some [4, 5] as a failure of the design process, especially of flight control system design. The problem is that in many cases, the effective aircraft dynamics and the associated flying qualities can be good right up to the instant that the A/RPC begins. The area where the design lacks is related especially to flight regimes where cliff-like phenomena are most likely to appear. Therefore, thinking in terms of vehicle modelling for RPCs, one has to build flight mechanics models capable of reproducing such cliff-like phenomena.

Unlike the airplane where, a six-degree-of-freedom (6-dof) rigid-body model is generally

enough to characterize the effective dynamics, in rotorcraft the classical 6-dof approximation is no longer applicable and depends on the rotor dynamics. Usually, the dynamics of the fuselage and rotor for an articulated helicopter can usually be seen as a cascade problem, i.e. a rapid rotor plane response followed by a slower fuselage response [6]. For hingeless rotor configurations, the body motion "speeds up" and the rotor dynamics "enters" into the 6-dof rigid body dynamics. It is well known for example that neglecting the flap regressive mode (representing the rotor disc-tilt dynamics) in a hingeless rotor actually means neglecting a very important oscillatory mode with short period frequencies. Also, [7, 8] demonstrated that modern rotorcraft with large hinge offset or hingeless rotors have increased coupling between the rotor plane dynamics and the body, resulting in a second-order initial response especially on the roll axis. Numerous couplings between the rotor and the body can occur in rotorcraft such as: the low-damped main rotor regressive lead-lag mode can be easily excited by cyclic stick inputs; the low frequency pendulum mode of external slung loads can be excited by delayed collective and/or cyclic control inputs. Other types of rotorcraft-centred deficiencies which might contribute to RPC belong to unfavourable conventional rotorcraft dynamics, such as lightly damped phugoid modes, or unfavourable roll attitude control/Dutch roll mode poles [98]. These were a problem in the past. With modem flight control systems these should not reappear as slow modes are readily suppressed by feedback. However, the category should not be abandoned, because novel aircraft dynamics with unusual configurations operating close to performance envelope limits could still be designed in the future [9].

The project did not advance much the state of the art in vehicle modelling; it rather improved the whole PVS system for RPC detection. Each partner employed its own helicopter modelling tool which was applied to the Bo-105 helicopter. This was a small multipurpose helicopter built by formerly MBB (now Eurocopter). It is currently out of service but its flight test data are now available and can be well used for model validation. Bo-105 was a highly manoeuvrable relatively small helicopter with a maximum gross weight of 2300kg. It had a four-bladed hingeless main rotor of 4.9m radius and a two-bladed teetering tail rotor. The composite blades of the main rotor had a very high equivalent hinge offset (non-dimensional flapping hinge offset equal to 0.1519) giving the Bo-105 an extremely high

bandwidth and excellent manoeuvrability in the roll and pitch axes. The pilot control inputs were augmented by two parallel hydraulic servo systems. There was no specific mixing unit, so that control inputs were only mixed at the swash plate.

Although the full scale Bo-105 was not prone to RPCs, the helicopter is a good example on how numerical degradation of its characteristics provokes unfavourable RPC. Delft University (TUD) model includes 16 states (6 translational and rotational body states, 3 flapping angles, 3 lead-lag states, 3 Pitt-Peters dynamic inflow and 1 quasi-steady tail rotor inflow. ONERA implemented the HOST model with 14 degrees of freedom (6 translational and rotational body states, 4 flapping states, 3 state Pitt-Peters dynamic inflow and 1 tail rotor inflow state). The University of Liverpool (UoL) model includes 44 states: 18 translational and rotational body states, 4 propulsion states and 22 rotor states, incorporating flap and lead-lag rotation for each individual rotor blade. The model is computed using a Peters-He 6 state Inflow model, with no built in correction factor. The model includes rotor stall, through dynamic look-up tables. No rotor interference is included in the model in its current form. The tail rotor is modelled as a Bailey type. Aerodynamic surfaces include non-linear effects, and stall.

Figure 2 presents the trimmed flight control and pitch and roll attitudes. All trimmed control positions for simulation models were found to reflect trends shown by the Flight Test (FT) data. It was also noted that all simulation models showed high correlation with results obtained in [10], where a similar modelling comparison process was undertaken in order to create a Common Baseline Model (CBM) of the Bo-105 for work within GARTEUR Action Group AG-06. For all trimmed flight control positions compared with the FT data, simulation models were found to be more similar to the CBM; for example the collective pitch was found to be $2°$ less than the FT data, lateral cyclic changes were found to be less pronounced in simulation models and, the increase in pitch attitude in the low speed regime was not captured by simulation models. A difference was found regarding the lateral trimmed control position of the TUD Bo-105 model. All models were found to capture the expected trend of lateral control deflection between 0 and 60 knots. Above this, the trend of the TUD lateral cyclic changes and deflection is found to increase with speed. ONERA and UoL models, along with the flight test data, show that lateral cyclic deflection

decreases with airspeed above 60 knots. This is likely due to the increased roll damping applied by the airflow. Tail rotor collective angle required for trim was found to be less for the UoL Bo-105 than ONERA and TUD models. Differences were found to be larger as speed increased. Results suggest that the tail rotor of the UoL Bo-105 is more effective than for other simulation models, as less pitch is required.

Figure 3 presents the on-axis and off axis rate responses to a longitudinal 3-2-1-1- input. One can see that pitch response is generally well correlated, however the off axis roll and yaw axes appear less well correlated.
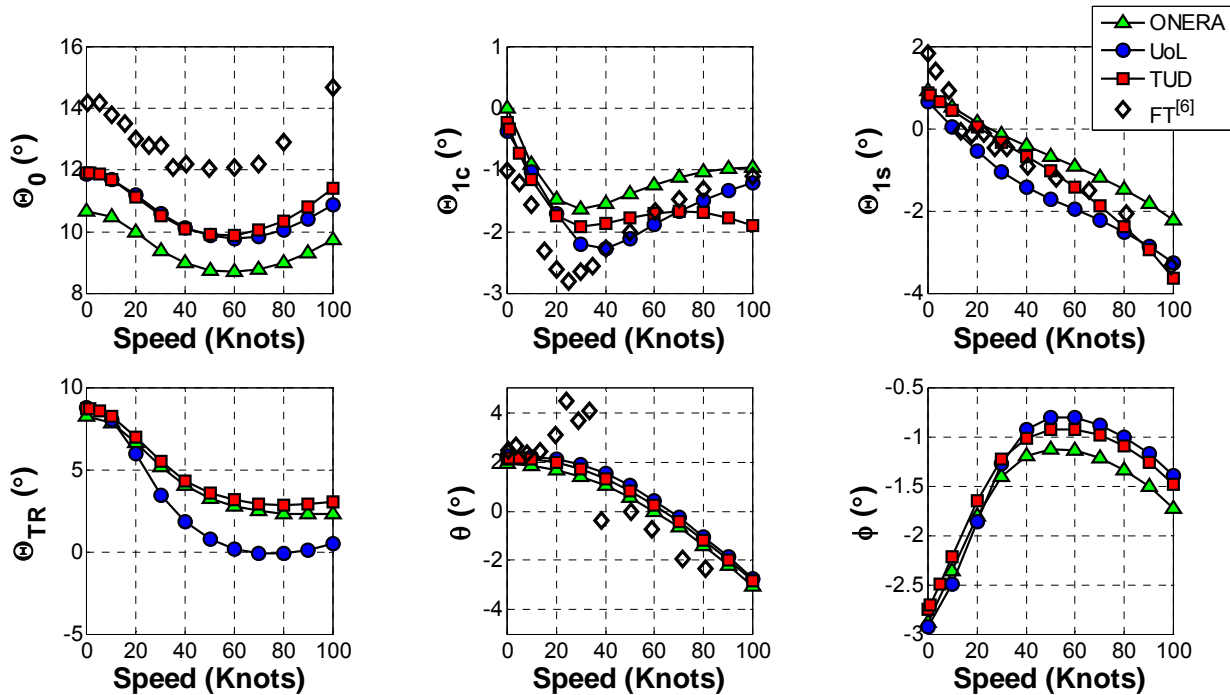
Figure 2 Trimmed flight control positions of the Bo-105 simulation models
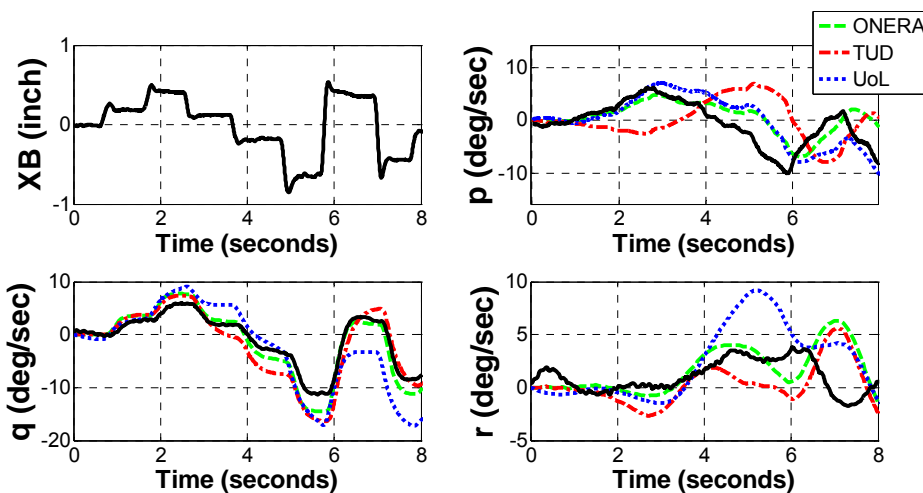
Figure 3 Bo-105 Simulation model responses to 3-2-1-1 Longitudinal Control and comparison to Flight Test data

A simple rate control with attitude hold control system (RCAH) was added to the model with the gains tuned to provide decoupled commands on the helicopter axes. A proper implementation of time delay contribution from flight control system coupled with the rotor-rigid body dynamics analysis is probably the next step in extending the flight models used in ARISTOTEL. This is because time delay is perhaps the "single biggest

problem" [11] for modern aircraft with high-bandwidth digital flight-control systems.

3. PILOT MODELLING FOR RIGID BODY RPC

3.1. Classical pilot modelling for PIO

Generally, in closed loop manual control systems, the human operator may have three main control strategies, i.e. compensatory, pursuit and precognitive behaviours [12]. "Compensatory" behaviour in the PVS system means that the pilot responds primarily to tracking errors displayed in the operator's compensatory display (see Figure 4); "Pursuit" behaviour means that the pilot response is conditioned on tracking errors plus system inputs/outputs. Precognitive behaviour corresponds to complete familiarity with the controlled element dynamics and the entire perceptual field where the highly-skilled human pilot can, under certain conditions, generate neuromuscular commands which are properly timed, scaled and sequenced so as to result in machine outputs which are almost exactly as desired. Precognitive behaviour is essentially open-loop. A special case of precognitive behaviour is synchronous behaviour. This means that, when the command input signal is sinusoidal the pilot can, after intermediate adaptation (which can include pursuit behaviour), duplicate the sinusoid without phase lag. The pilot dynamics can be modelled in this case as a pure gain. In a PIO-like instability, when the pilot has full-attention control, according to McRuer et. Al. [9], the behavioural patterns may be compensatory, pursuit, pursuit with preview (the response is conditioned on errors and system inputs/outputs and preview of the input is added), precognitive and precognitive/compensatory (dual mode control). To a first approximation, McRuer's [13] considered that in a fully developed PIO, especially for a large amplitude severe episode, either of Cat I and II PIO, the pilot dynamics transitions instantaneously to synchronous control, and the pilot is able to respond to the vehicle with open loop inputs based on an expected response. *"Synchronous behaviour is the most important type of pilot action for large amplitude severe PIOs" [9]*. A good approximation of the real pilot dynamics during PIOs is therefore a pure gain pilot model. During synchronous behaviour, the pilot duplicates a sinusoidal input signal with neither time delay nor phase lag. McRuer's assumption was supported by many analytical and experimental studies such as Gibson [5] and Duda [14].

The most elementary mathematical model for describing the compensatory/ synchronous pilot behaviour is the crossover model. Developed by McRuer and Krendel, Elkind and several others [15, 16], this model has often been used for RPC analysis. In the crossover model, the human operator is assumed to behave essentially linearly. The pilot behaviour is presented in the frequency domain in the form of a describing function. The pilot is assumed to be the controller in a time-invariant, single display, single control system, as shown in Figure 4. The describing function relates the pilot's output c to his/her visually observed input e. There are several excellent descriptions of this model in the literature. [15-17].
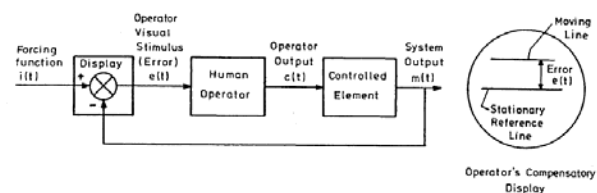

Figure 4 Compensatory Manual Control System

Under the restrictive condition that 1) the controlled element in the closed-loop –the aircraft- is assumed to be linear and 2) full operator's attention is assumed in performing a continuous compensatory tracking task. The crossover model has been applied in many PVS analyses, including those for RPC. A more recent application to the RPC problem was for a twin-engine medium class helicopter of Agusta Westland in hover and forward flight conditions at 40, 50 and 80 kts [18]. The crossover model was used also throughout the ARISTOTEL project for predicting Cat I and II rigid body RPC for a Bo-105 helicopter and also to provide realistic voluntary tracking error control in aeroelastic RPC analyses [19]. Examples of RPC predictions generated when using the crossover model will be presented in the next section. The results proved that its application to helicopter RPC is valuable.

3.2. Identification Techniques

As stated by McRuer [9] the problem of a pilot in an A/RPC is not due to his dynamic behavioural feature but due to the transition he/she may have between different behavioural patterns. *"Transitions in pilot behavioural organization are probably major sources of pilot-induced upsets which can serve as PIO triggers"* [9] For example, "a switch from pursuit' to compensatory operation can significantly reduce the available

bandwidth, with a concomitant expansion of system error, etc. According to McRuer [9], the types of transitions among the behavioural patterns which may occur in an A/RPC correspond to the so-called Successive Organization of Perception (SOP) Progressive Transitions" theory. According to this theory, the most common pilot behaviour shifts involved with PIOs appear to be transitions from full attention pursuit or compensatory operations in high-gain, high urgency tasks to a synchronous mode of behaviour. The pilot dynamics during the transition itself is, unfortunately, not well understood [9]. It is usually assumed that during the transition the pilot dynamics remain those adapted to the vehicle dynamics which were present before the change (so-called "post-transition retention" phase). The retention phase can last from one or two reaction times to many seconds [9].

To understand the characteristics of the pilot immediately before and after an A/RPC, ARISTOTEL conducted identification experiments to determine the pilot control strategy during a time delay triggered 'possible' RPC event for a hover stabilization task of a Bolkow Bo-105 rotorcraft simulation model [20] For this, a roll disturbance rejection single loop compensatory manual control task was flown in two simulators [20] in two phases presented in Figure 5 : Phase I before applying a time delay and Phase II after applying a time delay of 300milliseconds in order to trigger the RPC. Between these two phases there was the Post-Transition Retention phase in which the pilots still believe that they are controlling the vehicle operated prior to the change of control element dynamics followed by the pilots adaptation to the time delay applied in the controls . The disturbance forcing function was given to pilots as a sum of ten sinusoids between 0.061 Hz and 2.76 Hz. Figure 5 presents the frequency response of four pilots (A, B,C,D) in phase I and Phase II. . One can see that in Phase I Pilot C lowers the gain and "coincides" with pilot B, while pilot A and D keep almost the same frequency response. The results in Phase II show the adaptation of the pilots to the new situation. Looking at Figure 5 one can see that all pilots matched almost the same low frequency magnitude response with all various frequencies except Pilot D who showed a lower phase lag response at the lowest two frequencies than other pilots. This indicated that Pilot D noticed the reduced phase margin due to the applied time delay and tried to cope with it. Pilot A shows signs of a significant under-damped neuromuscular activation when compared to Phase I results.
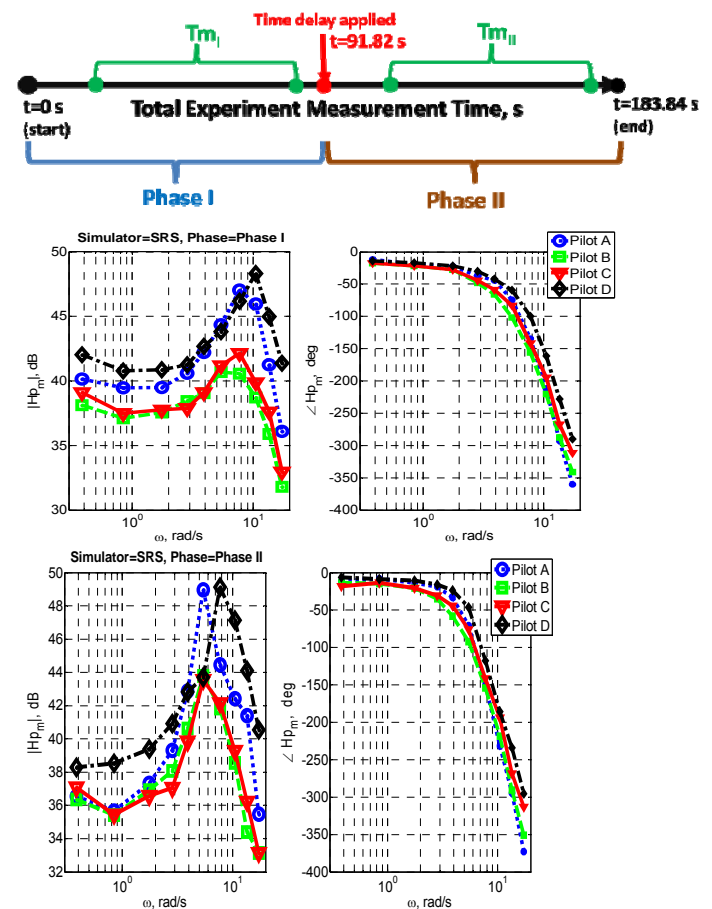

Figure 5 Measured pilot frequency responses for Phase I (before RPC) and Phase II (after RPC) in a roll disturbance task

The main adaptation of all pilots during the first experiment can be generalized as reduced gains and a small amount of lead around crossover frequencies, when exposed to a time delayed degraded controlled element. Concluding, the pilot adaptation when exposed to time delay could be summarized as: there is a tendency to reduce gains; there is a tendency to increase low frequency lead equalization in order to overcome the phase reduction caused by the additional time delay in the control path; there is a reduction in visual gains during possible RPC events, especially at low frequencies in order to increase stability of the PVS; there is a decrease in neuromuscular frequency, and attaining same pilot limitation, i.e. similar neuromuscular damping and pilot time delay. The identification methodology used above could be an important way forward towards understanding the pilot transition dynamics in an A/RPC.

3.3. Modelling the Boundary Avoidance Tracking Process - Gray's BAT Pilot model

The novel pilot modelling tools developed by ARISTOTEL for investigating A/RPC events relate to the so-called Boundary Avoidance Tracking concept (BAT) developed by Gray [21] for fixed wing aircraft and applied largely throughout the project by UoL and ONERA. Gray's main hypothesis is that during an A/RPC event, the pilot behaviour is different from the assumed point tracking (PT) flight behaviour and is more like tracking and avoiding a succession of opposing events which can be described as boundaries. GARTEUR HC-AG 16 performed simulator tests on BAT [42, 32] for a helicopter oscillatory pitch tracking task and in ARISTOTEL, UoL extended further the BAT research. Gray developed the BAT model, shown in Figure 6, and provided analysis techniques for estimating the associated boundary-avoidance model parameters [21].
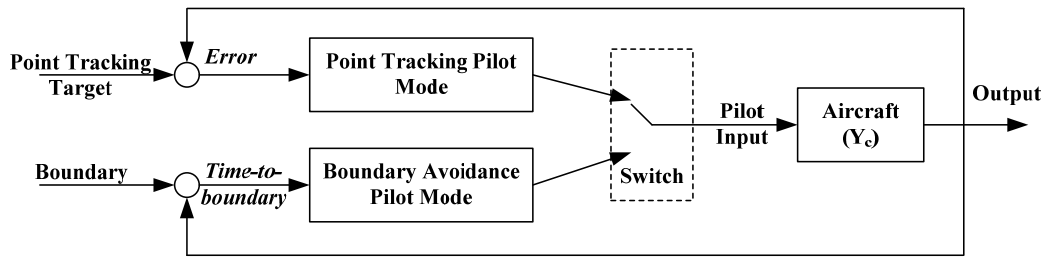

Figure 6 Gray's boundary-avoidance tracking model (based on [21])

The feedback loop includes both Point Tracking (PT) and Boundary Avoidance (BA) options with a logic switch/selector that assumes no transient; only one of the tracking channels is assumed to be operating at any one time. There are 2 boundaries in this particular model, designated upper and lower and only one can be tracked at a time. A key parameter in the BAT model is the time to boundary (τ_b) in Figure 6, based on the distance to boundary (x_b) at the current rate of approach ($\dot{x}_b$), defined as follows:

$$\tau_b = \frac{x_b}{\dot{x}_b} \qquad (1)$$

This parameter models the pilot's perception of the time-to-contact, introduced by Lee [22] as a development of Gibson's optical flow theory of visual perception [23]. However, it is clear that Gray independently discovered that the time to boundary was a key parameter in the pilot control strategy, without being explicitly aware of τ theory. The BA pilot model in Figure 6 is modelled as a BA feedback gain (K), dependent on the variable τ_b and the relationship is illustrated in Figure 7, in which the τ variable is shown in the conventional (negative) sense.
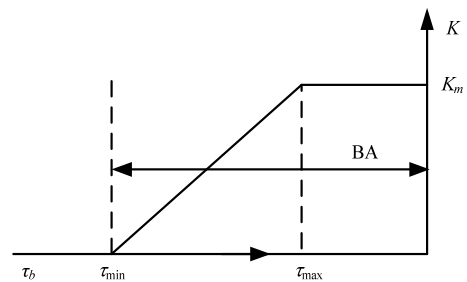

Figure 7 Feedback gain variation with the time to boundary (τ_b)

The BAT strategy is initiated when τ_b is lower (negatively) than the value τ_{min}. If the boundary continues to be approached, the feedback gain increases linearly to its maximum, K_m, in the form;

$$K = \frac{\tau_b - \tau_{min}}{\tau_{max} - \tau_{min}} K_m \qquad (2)$$

Using Eq.(2), Gray hypothesized that the control increases linearly as the boundary is approached

The BA pilot activity in Figure 6 is modelled as a pure BA gain (K) in Eq. (2). While the variation of this gain in Eq. (2) is linear, the essence of this operation is nonlinear, due to the dependence on $\dot{x}_b$ in equation (1). This brings with it a difficulty in analysing the stability of the closed-loop systems in Figure 6.

To address this issue, the BA process is modelled as the following form,

$$K(s) = (\tau_{min}s + 1)K_b X(s) \qquad (3)$$

in which K_b represent the BA control gain. Therefore, the BA feedback part of Gray's pilot model with the nonlinear τ variable can be approximately simplified into a lead perception term. The resultant closed-loop pilot model, including the vestibular and proprioceptive cues is illustrated in Figure 8.
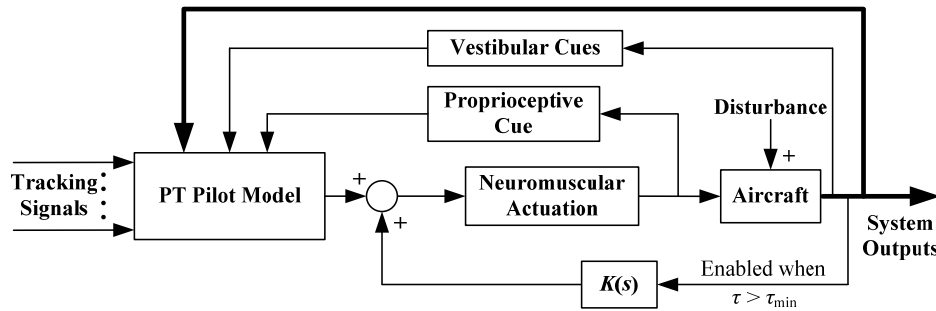

Figure 8 Closed-loop BAT pilot model with the modelled BA pilot part for tracking task

This rudimentary level of BA description from the derivation process, combined with Figure 8, shows the essential features in the study of BAT PIOs in this paper. First, the effect of the impending boundary is modelled as an additional positive inner feedback to the closed-loop system. This formula, in essence, describes the BA process as a disturbing influence created by the impending boundary, activated at the moment that $\tau > \tau_{min}$, on the primary (outer loop) pursuit task to which the pilot is, until that moment, giving full attention. The positive property of this feedback lies in that, with positive K_b, the resulting control effects will become larger as the detected boundary is approached (larger $X(s)$). Therefore, the stability of the closed-loop system pilot-vehicle dynamics can be changed and the BA process can therefore serve as a PIO trigger. The BAT-PIO onset detection can be estimated by analysing the effects of the inner linear BA perception-action form on the stability of the outer feedback loop system. Second, the structure in Figure 8 allows the investigation of the continuous contribution of the PT part of the pilot model, even after the BA process is triggered. This is different from previous work, which assumes that the PT and BA work independently, which does not reflect real pilot control activity in Figure 6. Overall then, the new structure appears to be an appropriate means to describe the pilot dynamics during the BAT process.

4. RPC PREDICTION

4.1. Theoretical RPC prediction

The prediction was made by applying existing criteria on one hand, and newly developed criteria and analysis tools on the other hand to the linearized helicopter models derived from the nonlinear BO-105 models. The flight conditions about which linearization is made, are hover, 60kts and 80kts forward flight. To create Category I PIOs proneness, added time delays are introduced to the models. To create Category II PIOs proneness, nonlinearities represented by actuators rate limits are added to the linear models.

4.1.1. Prediction based on traditional prediction criteria

Prediction based on Bandwidth-Phase Delay criterion

The RPC analysis was performed with the bandwidth-phase delay (BPD) prediction criterion while keeping the original boundaries applicable to fixed-wing aircraft. Figure 9 shows an example of application of the criterion to a Bo-105 helicopter during a pitch and roll tracking task flown from hover and 60kts initial flight condition when time delay was introduced in the pilot input (increasing from 0msec to 300msec). In this figure, the ADS-33 [38] Level 1, 2 and 3 handling qualities (L1, L2, L3) were plotted together with the PIO boundaries as defined for fixed wing aircraft for pitch axis responses. Looking at the figure, one can see that by increasing the time delay, the predicted handling qualities of the vehicle degrade, the bandwidth decreases and the phase delay increases making the helicopter RPC prone. According to ADS-33, only roll tracking task flown at 60kts with a time delay of 300ms is PIO prone. One can also see that the theoretical bandwidth/phase delay criterion results do not show strong dependency on flight speed. Furthermore, a

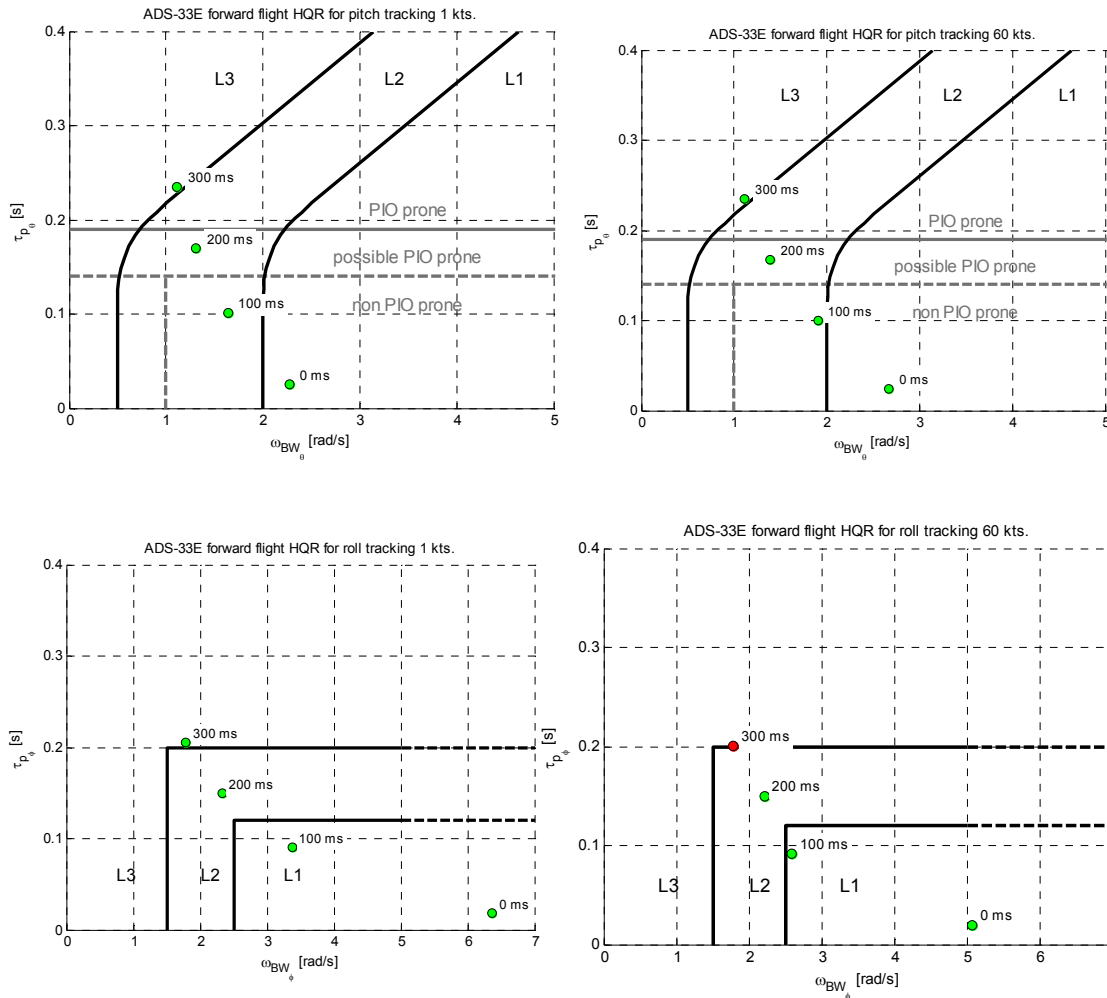relatively good agreement of the results from partners' models was found.

Figure 9 Bandwidth/Phase Delay criterion applied to the BO-105 helicopter in a pitch and roll tracking task flown from hover and 60 kts with various time delays introduced in the pilot stick

Prediction based on Open Loop Onset Point criterion

From existing prominent criteria to predict Cat II A/RPC for fixed wing aircraft, ARISTOTEL has applied the Open Loop Onset Point Criterion (OLOP) [14] for a range of roll and pitch tracking tasks (conducted in hover, 60 kts and 80 kts) performed with a rate command (RC) augmented BO-105 model when actuator rate limit was decreased.

The application of OLOP is dependent on three major factors: pilot model, rate limit, and stick input amplitude. The pilot model affects the general shape and position of the curve on the Nichols chart. The rate limit and input amplitude affect the position of the OLOP along that curve. The authors of OLOP suggested that the pilot be modelled as a pure gain because previous research has shown that a pilot acts as a simple gain during a fully

developed PIO (synchronous precognitive behaviour [12]). This gain has to be adjusted based on the linear crossover phase angle of the open-loop pilot-plus-aircraft system. Initially, the authors of OLOP suggested a crossover angle spectrum of –110deg (low pilot gain) to –160deg (high pilot gain) to evaluate pilot gain sensitivity. They also recommended using maximum pilot input amplitude when determining the onset frequencies. Clearly this is a worst case scenario although it is necessary to verify that this will not produce unreasonable results when compared to flight tests. As the original criterion often over-predicted the susceptibility of certain configurations to PIOs, the modified boundary OLOP2 derived from the original one by a 10dB gain shift.
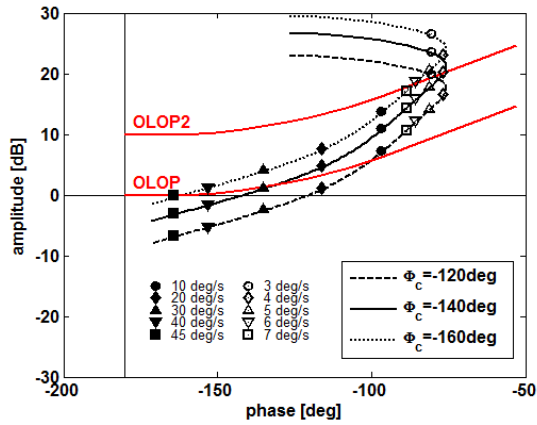
Figure 10 Roll axis OLOP at hover flight

Figure 10 shows an example of application of the criterion to a BO-105 helicopter during a roll tracking task at hover. For a pilot crossover phase angle $\Phi_C = -140 \deg$, the OLOP rate limit is 28.6deg/s with respect to the original boundary. With respect to the modified OLOP2 boundary, the rate limit is 4.1deg/s.
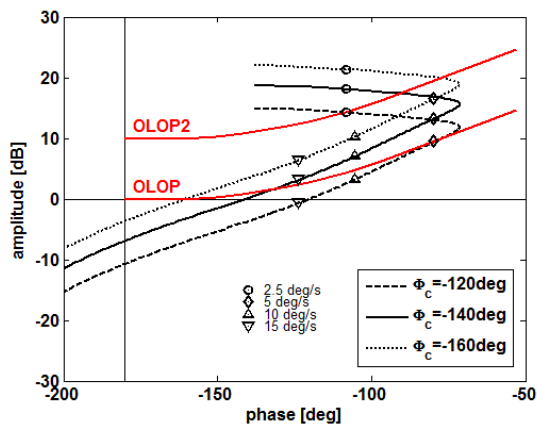

Figure 11 Pitch axis OLOP at hover flight

Figure 11 shows the application of the criterion to a BO-105 helicopter during a pitch tracking task at hover. For a pilot crossover phase angle $\Phi_C = -140 \deg$, the OLOP rate limit is 17.7deg/s with respect to the original boundary, and 2.7deg/s with respect to the modified OLOP2 boundary.

4.1.2. Prediction based on novel prediction and detection criteria

Prediction based on Enhanced Real-Time Oscillation Verifier

Original Real Time Oscillation VERifier (ROVER) was designed by U.S. army to warn pilots on the incipience and development of a RPC event by checking the pilot input and vehicle output magnitudes against predefined threshold boundaries [39]. ROVER operates on smoothed signals of two parameters, namely vehicle angular rate and pilot control stick input. Smoothing is performed using low-pass filters that remove high-frequency noise and data spikes. Throughout benchmarking and evaluation phases of this algorithm by TUD, it was observed that original ROVER had difficulties to accurately detect RPC occurrences during some segments of sample scenarios. To accomplish better detection accuracy, the original algorithm was improved by considering several peak selection adjustments [39] as illustrated in Figure 12 and Figure 13. After the stick input and aircraft roll rate are filtered, the algorithm determines the position of the "candidate" maxima and minima, as shown in Figure 12. Three consecutive points are needed to determine if a point is a candidate minimum or maximum.

Figure 12 Candidate maximum and minimum in ROVER algorithm

For selecting the peaks, an interval is used, so called peak selection thresholds (PST). If next candidate extreme is within the PST, in the classical algorithm the candidate is discarded and the algorithm continues. However, in TUD algorithm, all candidates are stored in an array and the resultant peak is calculated by averaging the candidate array. Thus, miscalculations of frequency and phase are reduced and a more robust peak selection was achieved. The difference between the two methods is illustrated in Figure 13.
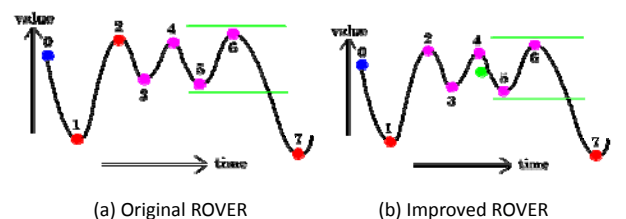

(a) Original ROVER   (b) Improved ROVER

Figure 13 Differences between the original and improved ROVER Time traces of a sample value for peak selection. Red dots indicate the candidate peak value. Pink dots indicate the discarded candidate points. Green lines show the PST boundaries. a) Original ROVER detection b) TUD detection adaptation, which shows the 'averaged' consecutive discarded candidates with a green dot

A further improvement to average peaking was introduced in TUD ROVER algorithm as

shown in Figure 14. The improvement consists of performing the averaging the stick input in the time interval until the body maximum or minimum is experienced. Therefore, the detection is carried to earlier stage of the PST limited interval detected peaks, as presented in Figure 14 by the green dot (improved average peak) showing an earlier detection than the claret red dot (original proposed average peak) and relating the peak of the pilot control to the corresponding body response. This improvement increases the efficiency of the adapted TUD ROVER algorithm in means of peak selection.
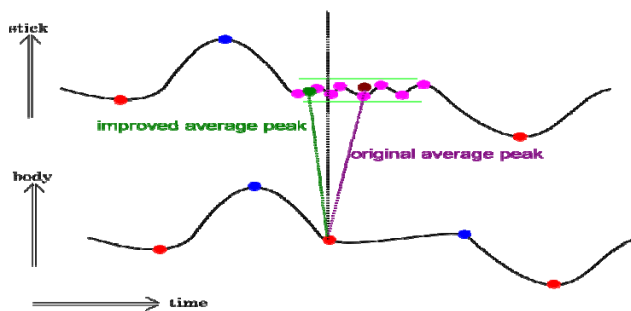

Figure 14 Peak averaging methods in ROVER algorithm

In addition to peak selection updates on ROVER, TUD also combined Handling Qualities (HQ) assessment of ADS-33 [38]. The scope of the integration of HQ into ROVER detection is to improve the pilot awareness due to incipience of a possible RPC by providing additional HQ degradation warning.

BPD criterion of ADS-33 was chosen to provide the HQ information. Briefly, this criterion checks the pilot control activity with the corresponding rotorcraft response and provides the level of HQ depending on the bandwidth and the resultant phase of the pilot control-vehicle system. Since ROVER explicitly checks for pilot control activity and the phase between control input and the body angular rate output, ROVER was adjusted to provide detection points superimposed on the BPD determination graph.

Prediction using the Phase-Aggression Criterion

Jones et. al. [41] proposed a new real-time detection for PIO, the so-called Phase Aggression Criterion (PAC). PAC achieves a 'detection' of an A/RPC through the observation of the Pilot-Vehicle System (PVS) phase distortion and the pilot input rate. Observing pilot input allows one to check that the pilot is coupled with the oscillations (a pre-

requisite for PIO) whilst the phase difference allows one to see whether the commanded input is in-phase with the vehicle response. The combination of the two parameters at a finite point in time allows one to objectively assess whether an A/RPC has materialised. The original parameter calculation, formulation of the algorithm and initial piloted simulation results are presented in ref. [41].

PAC was originally developed for observation of Category II PIO (due to quasi-linear system elements). Two test pilots completed a number of pitch tracking manoeuvres, awarding subjective opinion ratings. These subjective ratings, along with pilot comments and objective measures, were used to determine PIO susceptibility boundaries. These boundaries were then used to show at what stage pilots entered 'Moderate' and 'Severe' PIO conditions during the completed run. Comparison between ROVER was conducted throughout the investigation. Figure 15 shows a result from ref. [41]. This shows identified points determined using the PAC algorithm, for a completion of the pitch tracking manoeuvre. As shown in this case, clearly the vehicle has experienced resultant oscillations. PAC identifies these prior to the largest oscillations. Here, the result could be used to apply alleviation measures, to avoid the divergent PIO seen.
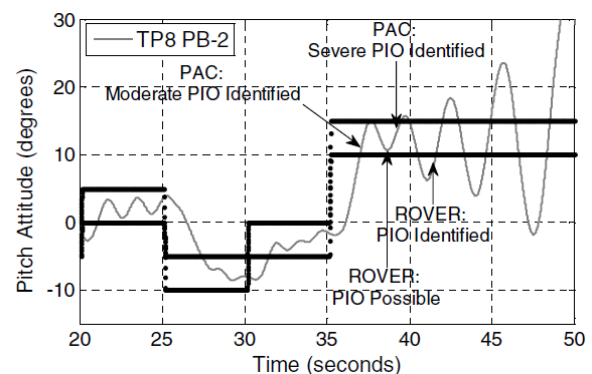

Figure 15 Example of PAC detection for a completion of the Pitch Tracking task

Based on results observed through the use of PAC, it has been proposed that it can also be used as a prediction algorithm (PRE-PAC). Rather than using a piloted simulation, a simple model of a sinusoidal input is defined. This is based on the important assumption that sinusoidal waves at maximum possible input amplitude with respect to frequency will be encountered by a pilot at some point. Therefore, rather than a sophisticated pilot model, the sinusoidal frequencies show what a pilot 'could' do. In order to use PRE-PAC one

needs first to pre-define input signals to be fed into a simulation model. These have been designed to account for a range of active pilot control inputs. Then, one needs to determine the time dependent 'Phase' and 'Aggression' parameters for each input signal, by running a simulation in the time domain. These results are then used to determine the systems incipience to RPC. The incipience is based on defined severity boundaries, which have previously been determined through a number of piloted simulation campaigns. These boundaries are presented on the Phase-Aggression chart, with some examples shown in Figure 16 to Figure 18. These examples show results from three linear vehicle roll models, for a rate command system. The shaded region represents the region of 'possible' pilot control, accounting for the range of control input frequencies applicable to PIO research (1-10 rad/s). For a given control input signal, one can determine the frequency dependent Phase and Aggression parameters. Moreover, one can determine whether these points are within the 'No PIO' region, 'Moderate PIO' region, or 'Severe PIO' region. Figure 16 shows a PIO robust roll model. Here, for all pilot control frequencies, results are within the 'No PIO' region. Figure 17 shows results from a model found to be incipient to 'Moderate' PIO. Here, the region of pilot control intersects the moderate PIO boundary at approximately 2.5 rad/s. However, a rapid reduction in change-in-phase following 5 rad/s means that the region does not intersect the 'Severe' boundary. Finally, Figure 18 displays results from a PIO prone case, whereby the region of pilot control intersects both the moderate and severe PIO boundaries. Here, the moderate boundary is crossed at 2.2 rad/s, and the Severe boundary at 3.1 rad/s.
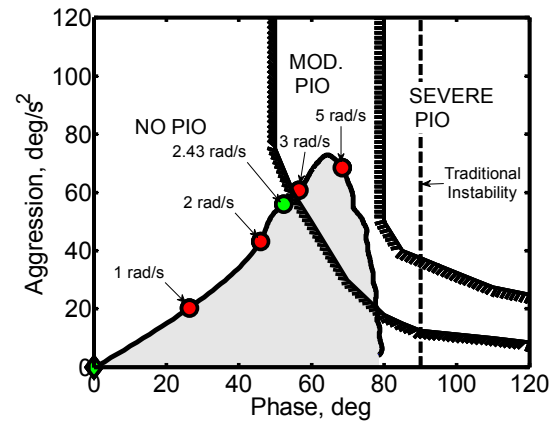

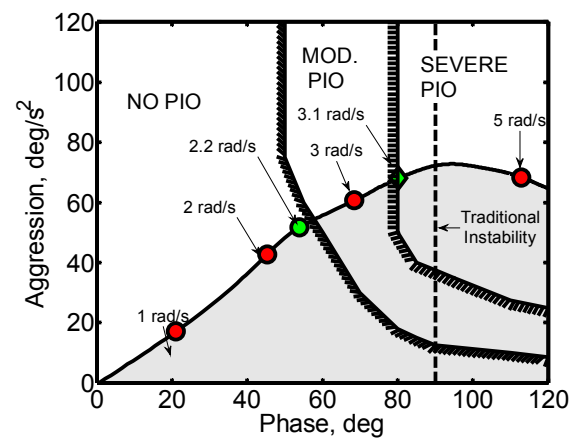Figure 16 Example of PRE-PAC Results for PIO Robust vehicle model, Lp = 10/s, τ=0ms

Figure 17 Example of PRE-PAC Results for PIO Incipient vehicle model, Lp = 2/s, τ=0ms

Figure 18 Example of PRE-PAC Results for PIO Prone vehicle model, Lp = 10/s, τ=0.3ms

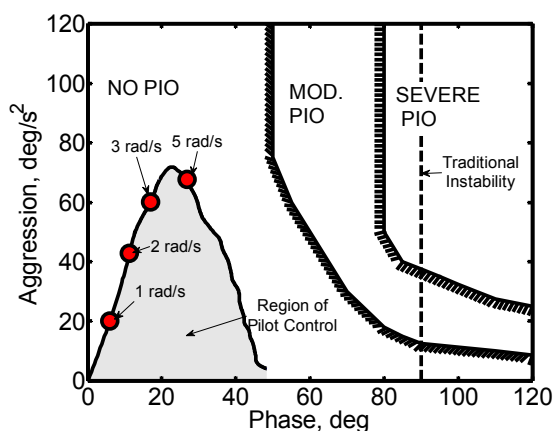To date, boundaries have been constructed to observe the incipience to Category I (linear) PIO for forward flight, roll-axis and for incipience to Category II (quasi-linear PIO) for roll- and pitch- axes.

The results from the application of PRE-PAC can be used in a number of ways. Firstly, results can be used to determine 'traditional' metrics indicating PIO susceptibility through a determined result. An example is to use the frequencies where the boundaries are intersected (termed the moderate and severe PIO trigger frequencies) to describe incipience. Another method is to use the results to 'map' the incipience to PIO against pilot input signal. For each PRE-PAC result, the pilot input is known, and one can determine the PIO incipience with respect to control magnitude and frequency. Results can be used to cross-reference pilot activity during flight, to see whether they reached necessary conditions to trigger PIO. This can provide validation, and explain why or why not a PIO has been experienced in-flight.

Prediction based on boundary avoidance tracking

The 3DOF longitudinal Bo-105 model linearized from the non-linear Bo-105 model [4] at 80 kts has been used for the investigation. The model is described as follows,

The 3DOF Bo-105 longitudinal model used in this paper is described as follows.

$$\dot{x}(t) = \mathbf{A}x(t) + \mathbf{B}\delta_{lon} \tag{4}$$

in which $x = \begin{bmatrix} u & w & q & \theta \end{bmatrix}$. The variable u is the x body axis velocity, w is the z body axis velocity, q is the pitch rate, and θ is the pitch attitude. The matrices A and B have the following values:

$$\mathbf{A} = \begin{bmatrix} -0.0397 & -0.0012 & 5.9132 & -28.9264 \\ -0.0149 & -0.8543 & 140.9837 & 10.7268 \\ 0.0082 & 0.0318 & -5.5064 & -4.0324 \\ 0 & 0 & 0.9997 & 0 \end{bmatrix}$$

$$\mathbf{B} = \begin{bmatrix} -1.0278 \\ -3.2261 \\ 1.2680 \\ 0 \end{bmatrix} \tag{5}$$

The neuromuscular damping ratio (ζ_{nm}) and natural frequency (ω_{nm}) in Figure 8 are selected as typical values of 0.707 and 10 rad/s, respectively [27, 28]. The actuator for the longitudinal control input is selected as [25]:

$$G_{ACT} = \frac{20^2}{(s+20)^2} \tag{6}$$

For the PT pilot model, the model structure used for the investigation is shown in Figure 19 (motion off) and Figure 20 (motion on).
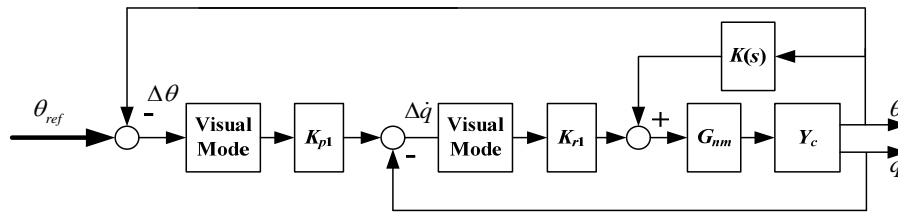

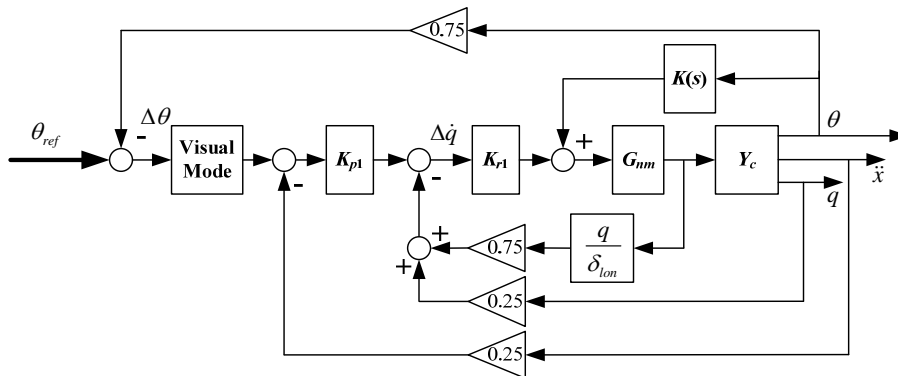Figure 19 Pilot model for 3DOF pitch tracking task (motion off)

Figure 20 Pilot model for 3DOF model pitch tracking task (motion on)

Here, θ and q are pitch attitude and rate responses to longitudinal stick input (δ_{lon}). The symbol $\ddot{x}$ is the surge acceleration. Compared with the simple form in Figure 19, the structure of Figure 20 provides more detailed information for pilot modelling. It actually represents a human pilot model that is now able to sense the available vestibular and proprioceptive cues which can be found in [25, 26]. The visual model is adopted on each visual channel to reflect the quality of visual information sensed by the pilot [26]. The transfer function in the proprioceptive feedback loop is suggested in [28] to be the lowest-order model that matches the pitch-rate response with the longitudinal input. Moreover, gain factors with a 0.75/0.25 split in Figure 20, as described in [27, 28], are used to weight the

degree of the importance of each information channel.

With the designed PT pilot, the closed-loop system stability in relation to the BAT phenomenon can now be investigated, subject to the variations of the 3 most interesting parameters: τ_{min}, K_b, and θ_d (boundary size).

The smallest critical K_b values (K_{bc}) that bring the closed-loop system (θ_{ref}/θ) to the neutral stability condition, with regard to various τ_{min} values (up to $-10s$). This is shown in Figure 21.
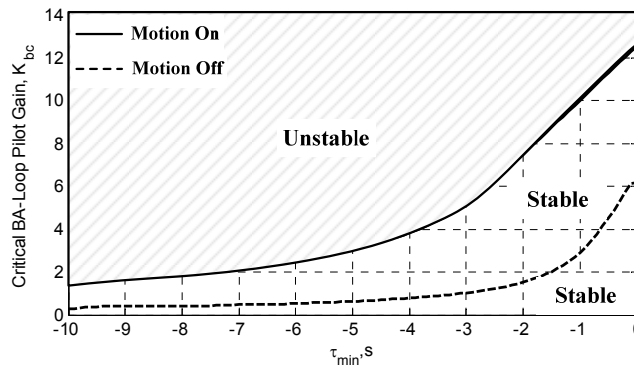

Figure 21 Stability regions with motion on and off against the BA initiation timing τ_{min}

Figure 21 is obtained with the τ_{min} range $(-10, -0.2 \text{ s})$. The selection of this τ_{min} region is based upon the findings of previous research [29, 30]. As shown by Figure 21, both K_{bc} curves have an approximately similar shape, but with a significantly improved stability region for motion on. Moreover, the stability-separation curves sharply increase as τ_{min} increases. This indicates, perhaps counter-intuitively, that the earlier the pilot initiates the BA process, the lower the level of control margin (the stable range of the gain K_b) will be available. This provides the pilot with less possibility of recovering from the influence of the approaching boundary. The primary reason for K_{bc} reducing as τ_{min} (negatively)

increases is due to the fact that this situation requires more pilot control effort to generate a lead equalized visual cue, leaving less control margin available for other tasks. The increased amount of lead requirement actually increases the effective time delay of the pilot-vehicle system [12, 13]. Under these situations, pilot performance can be significantly degraded.

The related open-loop ($\Delta\theta/\theta$ in Figure 19) crossover frequency (ω_c) and the open-loop neutral stability frequency (ω_u) where the open-loop phase angle is $-180°$ with regard to K_b and τ_{min} is plotted in Figure 22.
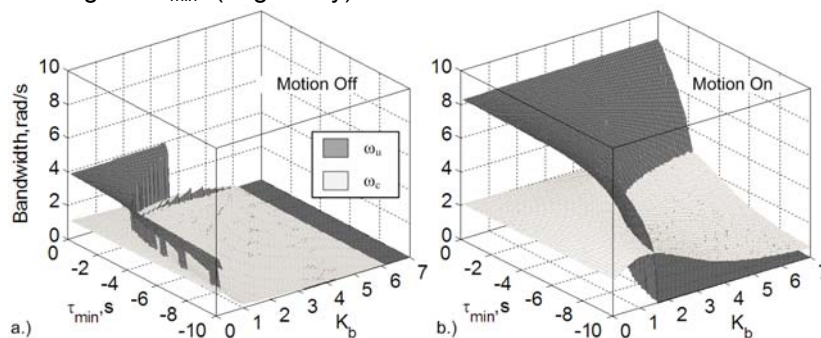
Figure 22 The bandwidth characteristic parameter variation with K_b and τ_{min}

Two features can be observed in Figure 22. First, the substantial influence of the inclusion of the BA loop can be immediately observed by the reduction of two bandwidth characteristic parameters, even reaching close

to zero, as K_b or τ_{min} (negatively) increases. The second feature, noted from Figure 22, is that the motion-on pilot-vehicle configuration achieves a superior stability performance, being improved by a factor of around 2. Its ω_c

curve surface initiates from 2 rad/s (at the left corner, K_b starting from 0.20), complying with the design objective, and then stays at this value over a large region of the parameter space until crossing the ω_u surface as K_b and τ_{min} vary. This is the opposite to what can be found in Figure 22a, where ω_c initiates from around 1 rad/s, even though it is designed to be 2 rad/s (without the BA loop, $K_b = 0$). This indicates that with motion on, the introduced BA loop has no significant influence on the pilot control activity (reflected by ω_c) and the consequent closed-loop tracking performance within this region. As K_b and τ_{min} increase, the ω_c surface slowly decreases but ω_u rapidly drops to zero.

The main reason for the stability region and bandwidth differences noted in Figure 21 and Figure 22 is likely to be due to the increased number of cues being available in the latter case (in Figure 20) i.e. the inclusion of the vestibular and proprioceptive feedback loops. [31] have found that the availability of these cues can be attributed to a reduction in the effective time delay and thus improved closed-loop stability performance because there is no need to generate angular rate or acceleration information by means of a lead equalized visual cue. The results above have demonstrated that the extra BA effort correlates with a reduction in the open-loop frequency bandwidths (in Figure 22) and the influence of the BA loop on the closed-loop stability and tracking performance equally increases the effective time delay. Taken together, the inclusion of the vestibular and proprioceptive feedback loops compensate for the penalty imposed by the addition of the BA loop.

The discussion above highlights the significant effects that the BA activity can have on the pilot-vehicle system performance. However, the investigation carried out so far only focuses on the stability of the system, without taking into consideration any boundaries or limits. The key facets of the BAT phenomenon stem directly from operational requirements and are hence mission-specific. Therefore, the results shown in Figure 21 and Figure 22 may be conservative in that the closed-loop system can be stable but its

response, depending on the type of input, may violate the boundary that could be considered to be a fatal error in normal flight operations (if the boundary happened to be the ground level, for example) [21]. Therefore, the boundary-constraint condition must now also be included in the investigation.

Figure 23 illustrates an idealized boundary avoidance tracking experiment, the pitch tracking task.
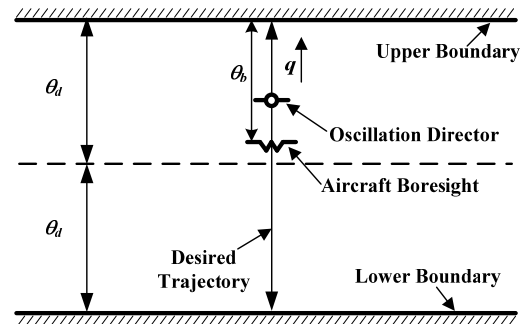

Figure 23 Illustration of a pitch tracking case with the boundary limits

The pitch tracking task of Figure 23 shows that the pilot (or pilot model) is required to command the aircraft bore sight symbol through the vehicle dynamics to capture a moving target (oscillation director), constrained within 2 boundaries. This is similar to a task flown in a simulation facility for an earlier investigation into rotorcraft pilot couplings, reported in [32]. For the purposes of this paper, the path of the director is composed of four sinusoids:

$$\sin(0.1\pi t) + 3\sin(0.05\pi t) + 2\sin(0.15\pi t) + 3\sin(0.3\pi t) \tag{7}$$

in order to try to reduce the 'predictability' of a single sinusoidal signal.

A series of boundary sizes, 6 - 15 deg, with an increment of one degree were selected for the investigation. The lowest boundary size takes the maximum amplitude (6 deg) of the desired combined signal in Eq. (7) into consideration. The fatal and safe regions under these boundary sizes are illustrated in Figure 24.
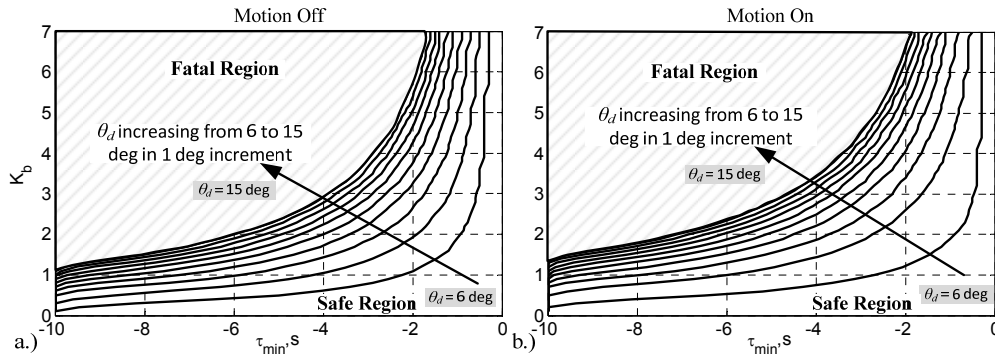
Figure 24 Fatal and safe region variation with boundary size for pitch model analysis

Figure 24 shows the profound influence of K_b and τ_{min} values on the safe flight region (entering into either system instability or violation of the boundary limit), subject to the various boundary sizes. These figures show that the safe K_b - τ_{min} regions within the designated boundary size become larger as the boundary size increases. This indicates the decreasing influence of the increased boundary size on pilot control activity. Four interesting features can be summarized from Figure 24. First, for the same τ_{min} value, the larger boundary size allows larger attainable pilot effort (K_b) and gives the pilot more control margin to avoid the impending boundary. This is especially reflected by the smaller τ_{min} values where there is no limitation on the K_b value that can be applied. This is actually a consequence of the BA process not being activated. The designed PT pilot model can ignore the boundary for a given boundary size where the τ_{min} values is relatively small (below a certain threshold). For example, for the designed experimental configuration, the boundary has no influence on the closed-loop tracking task when $\tau_{min} > -1.0$ s in the case of $\theta_d = 8$ deg, as shown in Figure 24. Moreover, the larger boundary size will result in a larger negative τ_{min} threshold. Second, compared

with those in Figure 24, the proposed stability curve in Figure 21 follows a similar shape, but appears to be too conservative, as expected, especially within the low τ_{min} range. The main reasons have been given above. However, the curve in Figure 21 is still useful because it illustrates the gross degree of the closed-loop system stability associated with the BA process, without requiring the prior knowledge of the desired tracking signal and the boundary size or other mission-specific details. Third, for the same K_b value, the range that the modelled pilot maintains safety will decrease as τ_{min} becomes negatively larger. This is reasonable in that for the same boundary size, the negatively larger τ_{min} means more lead-equalization effort is required. This will increase the effective time delay, as discussed above. Finally, the better closed-loop performance shown in Figure 21 and Figure 22, compared with each boundary size, is also reflected in the larger safer region in Figure 24.

With the derived safe region of Figure 24, the tracking performance for these boundary sizes is predicted in Figure 25. The tracking performance is defined as the root-mean-squared (RMS) difference between the desired (Ref) and simulated (Sim) pitch attitude responses.
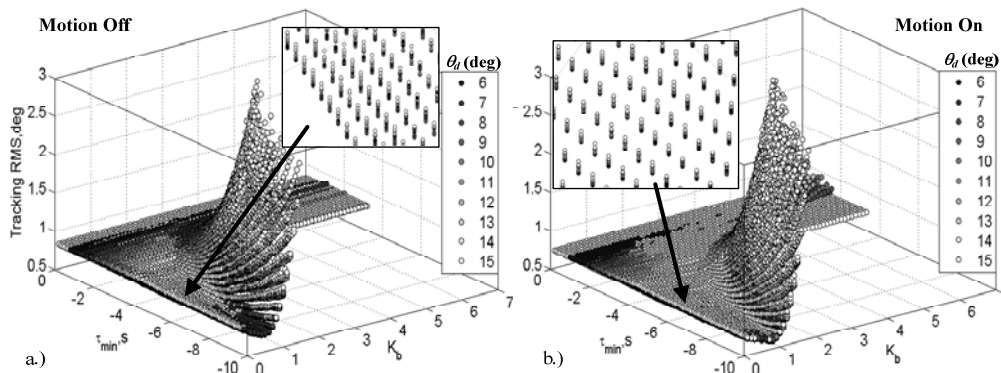

Figure 25 Tracking RMS variation with different K_b and τ_{min} values

18

Figure 25 shows the characteristics of the pitch tracking features under the variation of the boundary size. These can be summarized as follows. First, because the positive feedback property of the BA loop has a significant influence on the closed-loop stability in Figure 22 and Figure 24, it is expected that the larger positive feedback from the inner loop will result in a larger tracking error, arising from the reduced open- and closed-loop bandwidths. The distribution of the tracking RMS performance in Figure 25 confirms this expectation as K_b increases. This finding can be used to explain the phenomenon found in [29, 33, 34] for fixed-wing aircraft, whereby the tracking performance slightly improves as the boundary size decreases. Moreover, the previous study has assumed that, for the same task under the same flight condition, a pilot adopts the same τ_{min} value. As shown in Figure 24, the decreasing boundary size will compel the pilot to adopt a smaller K_b value to maintain safe flight which will in turn have a lesser effect on the outer closed-loop tracking performance. As a consequence, the smaller boundary size can actually increase tracking performance. This phenomenon is also reflected by the points within the region with the lighter shading in Figure 25 (those τ_{min} - K_b pairs in the common safe region in Figure 24). These points show that tracking performance slightly improves by approximately 5%, illustrated by a sampled zoomed area, as the boundary size decreases.

Second, the smaller boundary size results in a narrower safe region in Figure 24 and a worse tracking performance, shown by the darker region in Figure 25. Previous studies [29, 33, 34] also found that the tracking performance degrades when a certain 'critical' boundary size is reached and this can even lead to BAT-PIO situations. This primarily results from the reduced control margin for the smaller boundary size that makes the pilot more susceptible to system safety maintainability problems (i.e. a narrower safer region) as illustrated in Figure 24. If the boundary size is too narrow, for the same τ_{min} value, a small increase in K_b as the boundary approaches will cause a violation of the safe region.

Third, the two configurations depict a similar RMS-value distribution. However, the RMS values with motion on in Figure 25b , at the base of the distribution curve, are slightly improved by approximately 9% when compared with those of Figure 25a . This is to be expected since the frequency bandwidths associated with ω_c and ω_u of the motion-on configuration in Figure 22b are larger than those in Figure 22a. The larger ω_c values lead to better closed-loop tracking performance.

At the end of this section, three cases with τ_{min} = −2.0 and K_b = 3.0 with boundary sizes of 6, 10, and 15 deg have been selected, taking the tracking performance and closed-loop stability into consideration, to illustrate how the pilot model BA control effort varies with various boundary sizes. The simulation results with motion off and on are presented in Figure 26 and Figure 27, respectively. Figure 26 and Figure 27 show the significant influence of the impending boundary on the pilot control behaviour and the resultant tracking performance. The location of the selected τ_{min} and K_b values in Figure 24, for both configurations, predict that the case with θ_d = 6 deg will result in a failure situation (i.e. a boundary exceedance) whilst the other 2 cases will be successful. The results here have confirmed by these predictions. For the 6-deg case, the tight boundary results in pitch oscillations within the regions close to the boundary that are then quickly damped when the manoeuvre returns within the boundaries. This is consistent with Gray's model in Eq. (2) in that the BA process is excited only until τ_{min} is larger than a threshold value. Moreover, the observed decreasing influence of the BA on the outer-loop control activities when far from the boundary, analogously models the normally recommended strategy to address PIO situations i.e. to back out of the control loop [4]. Finally, the impending boundary introduces extra pulse-like pilot BA control effects and these further result in the severe variations in the pilot's longitudinal stick control (δ_{lon}). As the boundary size progressively increases, Figure 26 also shows that the resultant influence becomes significantly weaker (θ_d = 10 deg) and then quickly disappears after experiencing an initial influence (θ_d = 15 deg).

In addition to these similar results, the comparisons between Figure 26 and Figure 27 indicate that, for this tracking task, the motion and proprioceptive cues available have resulted in better tracking performance and less pilot control activity, in good agreement with the larger ω_c bandwidth in Figure 22.
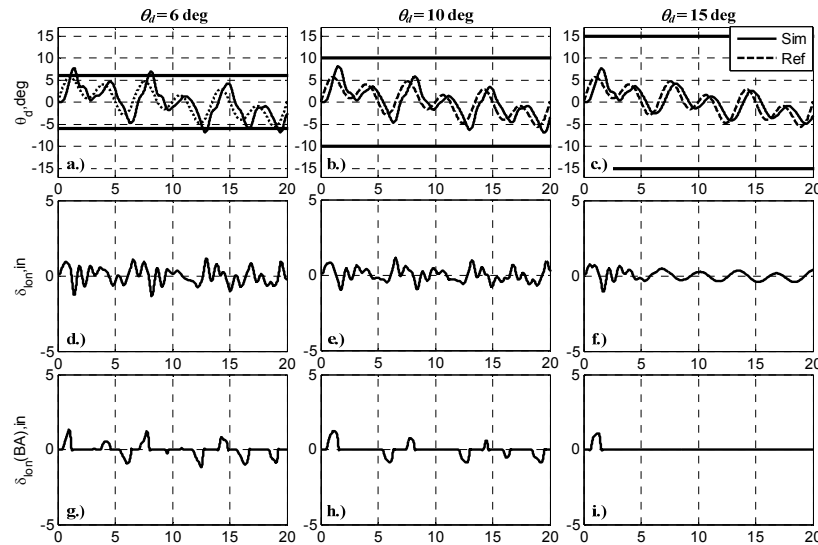
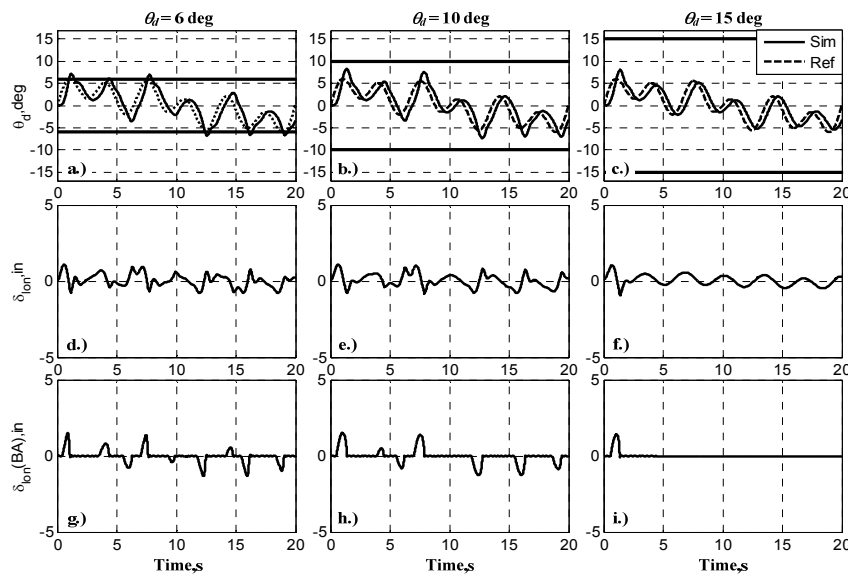Figure 26 Illustrating boundary effects with normal pilot aggressiveness (motion off, k_{agress} = 1)

Figure 27 Illustrating boundary effects with normal pilot aggressiveness (motion on, k_{agress} = 1)

Prediction based on optical tau

As stared above, the novel pilot modelling tools developed by ARISTOTEL for investigating A/RPC events relate to the so-called Boundary Avoidance Tracking concept (BAT) developed by Gray [21] for fixed wing aircraft. Also, in ARISTOTEL, UoL extended further the BAT connecting it to the "optical tau" concept. Tau theory is based upon the premise that purposeful actions are accomplished by coupling the motion under control with either externally or internally perceived motion variables. With the hypothesis that the pilot closed the aircraft

motion gaps by following a constant deceleration guide, the research bringing together optical tau and BAT has found that roll-step control (Figure 28) can be modelled as a prospective strategy by coupling lateral motion onto an intrinsic tau guide, taking the form of the constant deceleration, to fly the runway acquisition and tracking [41].

The results obtained have shown that the pilot initiates the deceleration when the time to the runway edge is around two seconds, regardless of the initial forward speed and height in both simulator and flight tests. This finding agrees well with the BAT initiation

timing value proposed by Warren's approach [30] through detecting the maximum control acceleration motion [41].

Figure 28 Roll step manoeuvre

In addition, the previous research [41, 43] has found that a strong correlation between motion and control activity exists. The deviations from the $\dot{\tau}$ constant strategy are manifest in variations in $\ddot{\tau}$ and are used to determine the BAT timing parameters, in contrast to the control acceleration variations proposed by other researchers. The values of $\dot{\tau}$ and $\ddot{\tau}$ at the target crossing can be used to establish the potential of a BAT event (the period a boundary contributes additional minor workload to pilot's control activity), or, more severely, a BAT PIO (a situation that a pilot cannot hold current main tracking tasks anymore). The hypothesized conditions are summarized in Figure 29.
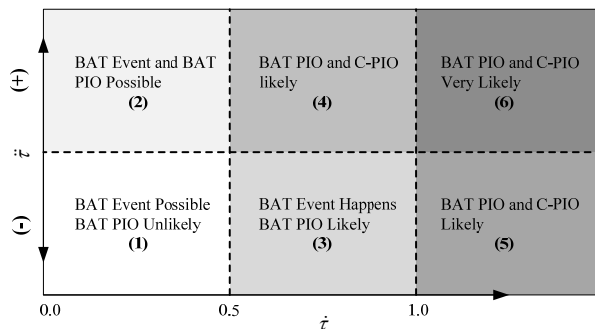

Figure 29 $\dot{\tau}$ and $\ddot{\tau}$ conditions for BAT event and BAT PIO prediction at the target (edge) crossing

Prediction based on Bifurcation analysis

Bifurcation theory considers the PVS nonlinear and therefore the motion of such system is composed of "fixed points" and "periodic orbits" ("limit cycles") [44, 45]. The stability of a fixed point and periodic orbit when a system's parameter is varied results in fixed-point and periodic orbit bifurcations. The different kind of bifurcations from fixed points and from periodic orbits is of interest for A/RPC study. A good explanation of bifurcation theory as applied to APCs is given in GARTEUR FM AG-12 [33]. Bifurcation theory

has been applied to APC analysis in refs. [46, 47, 48]. Mehra and Prasanth [47] considered two kind of nonlinear PVS, namely a linear airframe with a rate limited actuator and an airframe with nonlinear aerodynamics. The limit cycle amplitude was computed as a function of pilot gain, showing a large jump corresponding to the onset of nonlinear effects and PIO. Ref. BIF5 studied the PIO problem in the aircraft landing transition between the approach task and flare to touch-down. It was shown that, for a PVS system enhanced with a generic FCS, in highly demanding tasks such as the landing, too high at gain in the FCS reduced the pilot's allowable reaction time to levels where PVS oscillations appeared corresponding to a Hopf bifurcation.

The application of the bifurcation method in ARISTOTEL is aimed at predicting two types of RPC occurrences: Category II PIO due to rate limiting, and BAT RPC. The first step of the bifurcation analysis is the problem formulation: the PVS has to be formulated in a state-space form

$$\dot{X} = F(X, \lambda) \qquad (8)$$

where,

X is the n-dimensional state vector
λ is the m-dimensional parameter vector
F is a vector of n nonlinear continuous and differentiable functions.

The next step is the determination of the asymptotic behaviour of the system when the parameters of the system are varying quasi-steadily.

a)   Rate limiting

An approach similar to Mehra and Prasanth's [47] and GARTEUR FM AG-12's [46, 49] is used to assess PIO potential, with the following steps:

- Formulate a limit cycle and bifurcation problem for the PVS by augmenting the PVS with a nonlinear oscillator as the command input. Compute bifurcation surfaces and limit cycles as a function of pilot gain and rate limit.

- Check for Hopf bifurcations and jump resonances leading to limit cycles and large jumps in limit cycle amplitude as the pilot gain increases. Flying qualities "cliffs" are associated with these nonlinear phenomena.

21

The rotorcraft model used is the linearized helicopter models derived from the nonlinear BO-105 models implemented in SIMONA (TUD), HELIFLIGHT-R (UoL) and HOST (ONERA). The pilot model used is a crossover model with a pure gain. This assumption is well accepted in the case where the PIO is fully developed (synchronous precognitive behaviour). The closed-loop model of the PVS is presented in Figure 30, including the limitation on the stick deflection and the rate limit element. The PVS is augmented with a command signal generator, represented by a nonlinear oscillator which has the periodic command as an asymptotically stable periodic solution. Indeed, as the PIO must be predicted for any initial conditions, a nonlinear oscillator is required. In state-space form, the proposed oscillator is given by

$$\dot{x}_1 = A^2 x_1 + \Omega x_2 - \left(x_1^2 + x_2^2\right) x_1$$
$$\dot{x}_2 = -\Omega x_1 + A^2 x_2 - \left(x_1^2 + x_2^2\right) x_2$$

(9)

where Ω is the command input frequency and A is the command input amplitude.
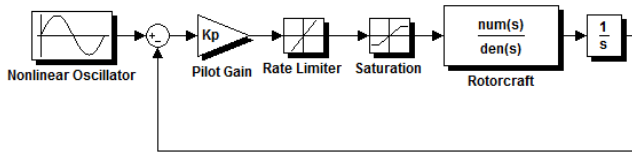

Figure 30 Augmented PVS for Cat II analysis

It should be noted that the command signal does not correspond necessarily to real piloting tasks intended to trigger PIO, but it constitutes a mathematical trick to make possible the use of standard bifurcation methods. Practically, the worst case should be retained for the command signal. As there is no feedback from the PVS to the oscillator, it can be shown that the global properties of the PVS are the same as those of the augmented system. The augmented system is an unforced dynamical system and can be analysed using standard bifurcation methodology.

The amplitudes of the limit cycles are determined as functions of the rate limits and the pilot gains. The pilot model gains are assumed to be adjusted based on the linear crossover phase angle of the open loop rotorcraft-pilot system Φ_C. Within this study a gain spectrum from $\Phi_C = -110 \deg$ (low pilot gain) up to $\Phi_C = -160 \deg$ (high pilot gain) is used. A metric is proposed to measure the PIO

susceptibility, given by the derivative of the amplitude of the rotorcraft limit cycle with respect to the rate limit, i.e. $\partial q / \partial r_{\lim it}$ in the pitch axis, and $\partial p / \partial r_{\lim it}$ in the roll axis. It can be interpreted graphically as the slope of the limit cycle amplitude envelope [49]. A sample of the prediction results is presented below with the following formats: 3D plot of PIO susceptibility parameter versus rate limits and pilot gains, 2D plot contour of PIO susceptibility parameter.
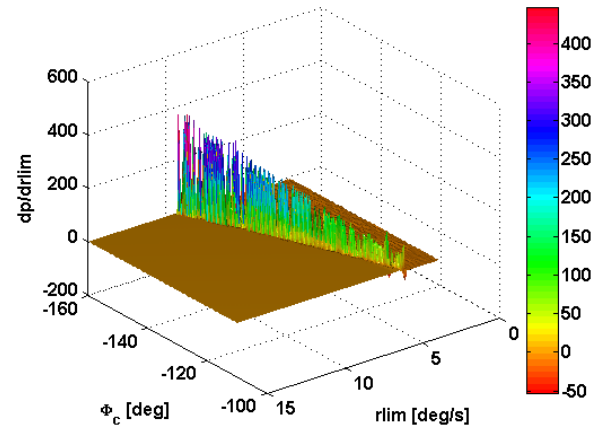

Figure 31 PIO susceptibility parameter in roll as a function of rate limit and pilot crossover phase angle
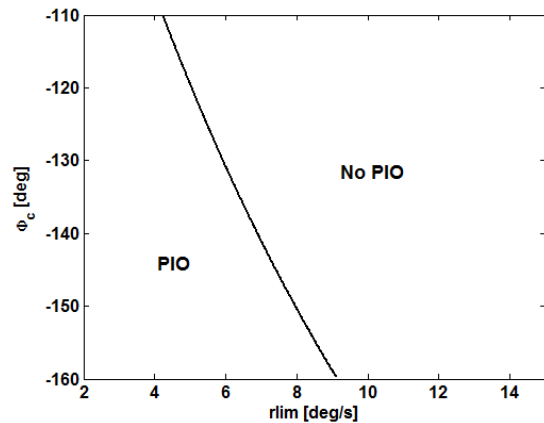

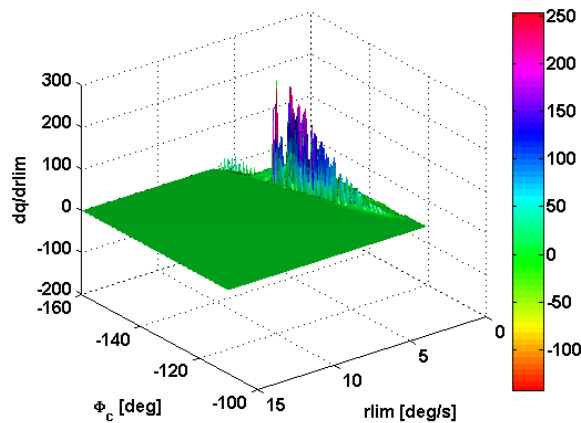Figure 32 Roll PIO boundary based on PIO susceptibility parameter

Figure 33 PIO susceptibility parameter in pitch as a function of rate limit and pilot crossover phase angle
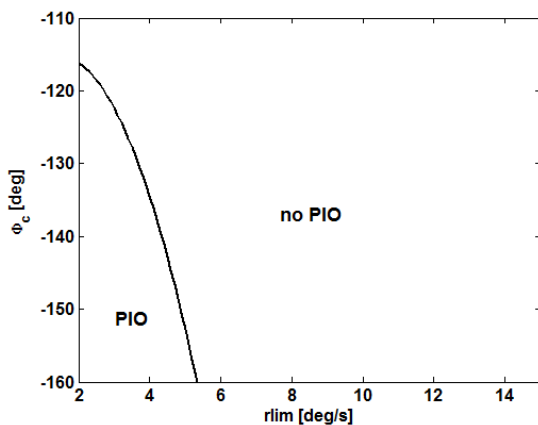

Figure 34 Pitch PIO boundary based on PIO susceptibility parameter

For high rate limits, the amplitude of the PVS system is that of a periodic solution, depending on the command frequency and amplitude. As the rate limit decreases, a Hopf bifurcation is encountered leading to large jumps in amplitude and limit cycles illustrated by discontinuities in roll derivative $\partial p / \partial r_{\lim it}$ (Figure 31), or pitch derivative $\partial q / \partial r_{\lim it}$ (Figure 33). The combinations of pilot gains and rate limits for which a large jump in limit cycle amplitude is observed are plotted in Figure 32 and Figure 34 as boundaries delimitating regions where the rotorcraft is PIO prone and PIO free. For example, for a pilot crossover phase angle $\Phi_C = -140 \deg$, this can be already observed for rate limit 6.7deg/s in roll and 4.3deg/s in pitch.

b) Boundary Avoidance Tracking

The emphasis in this type of RPC occurrences was on predicting RPC due to switching control modes between Point Tracking (PT) and Boundary Avoidance Tracking (BAT). The tracking manoeuvre considered is a roll step manoeuvre described as follows: the helicopter is initially flown along one edge of a runway. The piloting task consists of traversing the runway to reach the other edge over a specified distance and fly through a series of gates (the boundaries). Using Gray's model [21], it was searched the combinations of the model parameters that drive the pilot-vehicle system into instability. Gray's model parameters are, the minimum time to boundary Tmin at which the pilot starts to respond to the boundary, and the maximum time to boundary Tmax at which the pilot applies the maximum boundary gain to avoid reaching the boundary. Figure 35 presents the combinations of Tmin and Tmax which delimitate regions of stable/unstable motion based on the analysis of the asymptotic behaviour of the closed loop pilot-vehicle system.
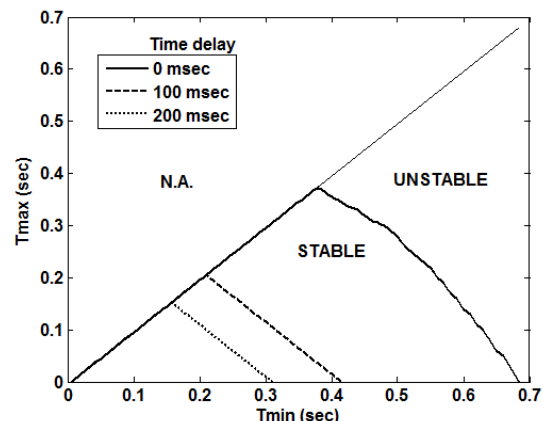
Figure 35 Bifurcation surface of a PT/BAT pilot-BO-105 system performing a roll step manoeuvre. Influence of additional time delay

According to the definition of Tmin and Tmax, one has to consider only the area on the figure corresponding to Tmax<Tmin. The straight borderline Tmax=Tmin represents a pilot who switches instantaneously from the PT mode to the BAT mode as time to boundary decreases, while the borderline Tmax=0 (i.e the Tmin-axis) represents a pilot who proceeds gradually. Any point inside the area delimited by the bifurcation surface is stable. It is evident that a real pilot will not keep constant Tmin and Tmax but will adopt rather an adaptive strategy. The bifurcation method which is based on the analysis of the asymptotic behaviour of the closed-loop pilot-vehicle

system cannot predict this strategy nor the effects due to transients. However, as long as the strategy leads to a combination of (Tmin, Tmax) inside the region of stability, the system is expected to be BAT RPC free. The influence of additional time delay on the region of stability is also presented on the figure. As expected, increasing the time delay reduces the region of stability.

4.2. Verification of theoretical RPC prediction

The data and PIO Ratings (PIOR) collected during the 1st test campaign on the SIMONA and the HELIFLIGHT-R simulators were used for the assessment and validation of off-line RPC prediction criteria and on-line RPC detection algorithms.

4.2.1. Verification of Off-line RPC prediction criteria

To assess the off-line prediction criteria, the correlation procedure compares the number of cases predicted by each criterion to be PIO prone/free to the actual number of simulator test PIO as shown in Table 2.

Table 2. Evaluation of PIO prediction

Number of cases		Simulator test PIO	
		NO PIO	PIO
PIO prediction	NO PIO	B	A
	PIO	C	D

From this table:

- B is the number of "Pass" cases where both prediction and experimentation agree.
- D is the number of "Fail" cases where both prediction and experimentation agree.
- A is the number of predicted "Pass" cases which "Fail" during the experimentation.
- C is the number of predicted "Fail" cases which "Pass" during the experimentation.

The conventional PIOR scale was used by the pilots to evaluate PIO susceptibility. From that scale, the following correspondence is applied to discriminate the "Pass" cases and the "Fail" cases:

- "Pass" corresponds to PIOR 3, i.e. absence of oscillations

- "Fail" corresponds to PIOR>3, i.e. presence of oscillations.

The effectiveness of the PIO criterion in predicting PIO can be evaluated according to the following performance metrics:

- Global success rate I1 = (B+D)/(A+B+C+D) i.e. the percentage of cases which are correctly predicted to be PIO free or prone.

- Index of conservatism I2 = D/(C+D) i.e. the percentage of cases predicted PIO prone which have actually undergone PIO in reality with respect to the total number of predicted PIO prone cases.

- Safety index I3 = D/(A+D) i.e. the percentage of cases which are predicted by the criterion to be PIO prone, with respect to the total number of simulator test PIO cases.

The performance metrics obtained for the different prediction criteria are given below per axis and per task.

Verification of Bandwidth-Phase Delay criterion

As prediction was made for each axis separately (pitch or roll), it was chosen the manoeuvres that solicit mainly one axis to validate the criterion

- Roll axis: roll tracking task and side step manoeuvre

- Pitch axis: acceleration-deceleration manoeuvre

Table 3. Assessment of BPD prediction

Tasks	I1	I2	I3
Roll tracking	70%	16%	25%
Roll step	80%	60%	66%
Acceleration-deceleration	82%	33%	100%

In the roll axis, while there is a good pilot rating trend with time delays less than 200ms, the scatter of the PIOR for time delays between 200ms and 300ms does not allow a definite validation of the boundary. For example, in the roll tracking task, 5 out of 6 runs of the 300ms time delay-configuration obtained better PIOR than 2 out of 4 runs of the 200ms time delay-configuration. One reason that can be attributed to this result a priori inconsistent according to the predictions is that the pilot gain was not high enough. The correlation is better for the roll step manoeuvre than for the roll tracking task.

In the pitch axis, a 0% success rate index is obtained for the 200ms time delay-

configuration. By shifting the phase delay boundary from the actual value of 0.19 sec to 0.22 sec, the success rate will become 100%. However as the number of runs was very small for this configuration (as well as for the 100ms and 300ms time delay-configurations), correlations have to be made with more experimental data.

Verification of OLOP criterion

As prediction was made for each axis separately (pitch or roll), it was chosen the manoeuvres that solicit mainly one axis to validate the criterion
- Pitch axis: pitch tracking task
- Roll axis: roll tracking task

The assessment of the OLOP criterion is dependent on the pilot gain. However in the correlation procedure, it was assumed a fixed pilot crossover phase of -140deg.

Table 4. Assessment of OLOP prediction

Tasks	I1	I2	I3
Pitch tracking	80%	62%	83%
Roll tracking	93%	-	0%

In the pitch axis, there is a good pilot rating trend with all rate limits.

In the roll axis, the very low number of runs (2) for the 5deg/sec rate limit-configuration does not allow a significant assessment of the criterion for that configuration. The bad safety index is due to the fact that while the criterion predicts no PIO, one run was awarded PIOR 1 and the other PIOR 4. However, it can be seen in Figure 10 that the 5deg/sec rate limit configuration is very close to the OLOP2 boundary. In general, a refinement of the criterion assessment can be obtained through a preliminary identification of the pilot gain.

Verification of Phase-Aggression criterion

Validation of the boundaries was performed for both manoeuvres where rate limiting was used during the 1st Rigid Body Test Campaign; Pitch Tracking and the Acceleration-Deceleration.

All test points, for which the pilots had awarded subjective opinion ratings, were processed using PAC. Results from analysis of the Pitch Tracking task are shown in Table 5.

Table 5. Assessment of PAC prediction

Tasks	I1	I2	I3
Pitch tracking	81%	60%	86%
Acceleration-deceleration	83%	89%	80%

For the pitch tracking task, the majority of test points presented 'no PIO' that was detected by the pilot and/or the PAC boundaries. However, for the majority of cases where the pilot detected PIOs, the PAC boundaries also showed PIO detection. The correlation was not as strong as hoped, with a number of disagreements when pilots subjectively believed they had not entered into PIO. It is believed that for the most part, incorrect judgement by the pilot, using the PIO rating scale had the largest effect on the differences obtained. Detailed results with respect to the rate limit values used show that PIOs were not detected by PAC and the pilot until a rate limiting value of 2.5deg/s. This is consistent with OLOP predictions shown in Figure 11.

Results from the analysis of the Accel-Decel task show that a good correlation between the pilot subjective and the PAC detection boundaries was found. For all test points, only 3 disagreements were found. As with the Pitch Tracking task, clear PIO potential was found with rate limiting of 2.5deg/s.

Verification of Bifurcation analysis

Validation of the analysis was performed for the same manoeuvres used to assess OLOP, i.e. the roll tracking task and the pitch tracking task. Like OLOP, the assessment of the OLOP criterion is dependent on the pilot gain. However in the correlation procedure, it was assumed a fixed crossover phase of -140deg.

Table 6. Assessment of bifurcation analysis

Tasks	I1	I2	I3
Pitch tracking	80%	62%	83%
Roll tracking	93%	50%	50%

In the pitch axis the performance of the bifurcation analysis is comparable to OLOP.

In the roll axis, the very low number of runs (2) for the 5deg/sec rate limit-configuration does not allow a significant assessment of the method for that configuration. The safety index is equal to 50% due to the fact that while the criterion predicts a PIO prone configuration, one run was awarded PIOR 1 and the other PIOR 4.

Verification of Enhanced ROVER

The enhanced ROVER was used on the measurement data recorded from the first Rigid Body Test Campaign (RBTC) tasks, particularly the data from roll tracking task. Roll tracking task was chosen as a case study

because the task was single axis with a linear rotorcraft model, which eases the analysis. Moreover, only the measurement data of test matrix configurations with applied "time delays" were used. The reason to select those configurations is due to achieving a linear triggering effect and easiness of HQ determinations. Enhanced ROVER detected RPCs and corresponding HQ levels according to BPD criterion are plotted in Figure 36 with awarded HQRs and PIORs of pilots.
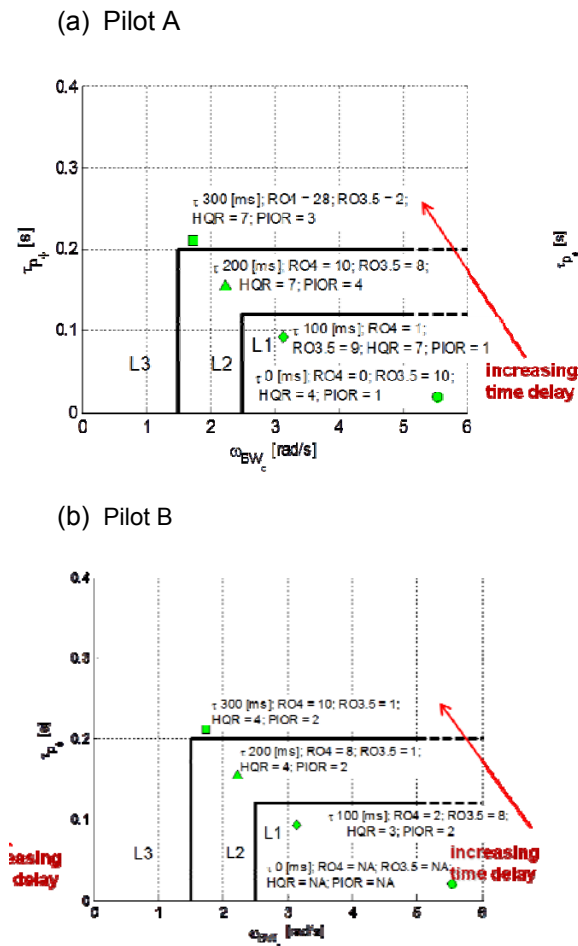
(a) Pilot A

(b) Pilot B

Figure 36 Bandwidth phase delay criterion with detected ROVER flags (RO4=4 flags, RO3.5= Warning flags), HQR and PIOR of Pilot A and Pilot B during roll tracking task of first RBTC with various time delays

It is shown in Figure 36 that with increasing time delay, HQ of the vehicle degrades and ROVER can detect more RPC occurrences and warnings. However, pilot ratings show that pilot B did not report any of the time delayed configuration as PIO according to PIOR scale and awarded the same PIOR for all configurations. Moreover, according to subjective ratings of pilot B for 100, 200 and 300 ms time delayed configurations, it can be concluded that he perceived that there was a

noticeable HQ degradation for 200 ms delayed from level 1 to level 2 (HQR 3 to 4 respectively), whereas BPD criterion shows a continuous HQ degradation with increasing time delay, as shown in Figure 36 Pilot A showed a similar consistency in his HQRs, level 2 (HQR 4) for no time delay and a constant level 3 (HQR 7) for 100 to 300 ms time delayed version. On contrary to pilot A, pilot B awarded noticeable PIO (PIOR 4,3) for 200 and 300 ms delayed configurations.

4.2.2. Verification of BAT Pilot Model Using Piloted Simulation

Discussion on Model Predictions

Based upon the results of the modelling and simulation exercise above, a number of predictions can be made about the way that a pilot might be expected to behave when confronted with a point tracking task that becomes a boundary avoidance type task either in flight or, more particularly, in a simulation environment. First, it would be expected that there would be a difference in both the observed control behaviour and tracking performance between test points with any motion cueing system switched on and switched off (or no motion cueing system available). Furthermore, the tracking performance with motion off is likely to be more inconsistent between test points than with motion cueing on (based upon the sharp roll off of bandwidth in Figure 22). Second, it would be expected that tracking performance would vary with the size of the time to go to any boundary to be avoided. The variation may be better or worse with, say, decreasing boundary size, but this is dependent on both pilot gain and the moment that the pilot responds to the boundary itself (see Figure 25). Finally, the modelling exercise indicates that BAT PIOs will be difficult to initiate but that they should be easier to trigger with any available motion cueing off. Figure 22 shows some high BA control gains required for instability to occur but that the required bandwidths would be lower, and closer to typical achievable pilot values for motion off cases. Once a BAT PIO is initiated however, it should occur around the frequency ω_u. In order to test these predictions, a simulation experiment was conducted. This Section reports on that experiment and compares its findings with the theoretical study reported thus far.

Description of Experimental Set-Up

The experimental study was conducted using the HELIFLIGHT-R simulator at The University of Liverpool [35]. The external and

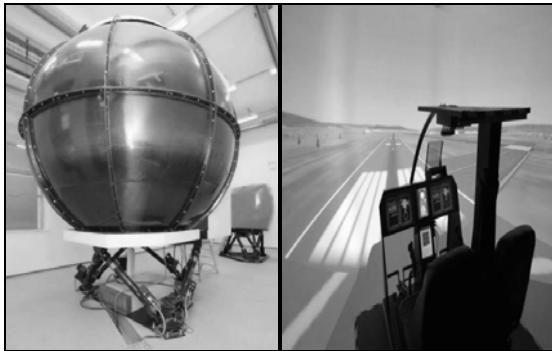interior views of the simulator are shown in Figure 37.

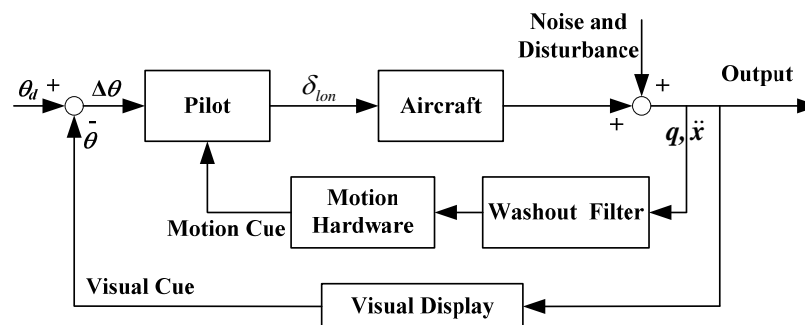Figure 37 The external and interior views of HFR

Figure 38 Diagram of pilot-in-the-loop simulation in the HELIFLIGHT-R simulator

The following should be noted in relation to Figure 38. First, the same aircraft model and pitch tracking task as for those used for theoretical analysis in Section IV were implemented. Therefore, during the simulation process, only the longitudinal control channel was available to the pilot, the other three (lateral, collective, yaw pedals) had no influence on the model response. Because of the available vertical field-of-view in the HELIFLIGHT-R simulator, the maximum boundary size used for the experiment was 12 deg, as opposed to the 15 deg used for the theoretical investigation. Second, for the motion-on configuration test points (consisting of the motion system hardware and washout filters illustrated in Figure 38), only the surge acceleration ($\ddot{x}$) and the pitch rate (q) were fed to the motion base drive algorithms. This is consistent with Figure 20. Finally, the pilots were instructed to focus on the head-up display (Figure 23) that showed the tracking task symbology and to ignore the head-down

The proposed closed-loop BAT model of Figure 20 was configured to represent the task conducted in the HELIFLIGHT-R simulator as shown in Figure 38.

display panel during the task. The external visual environment was severely degraded by a simulated visual representation of a thick fog. This minimized the possibility of the pilot being distracted by other objects in the visual scene. All of these measures were undertaken to try to ensure that the only visual cue available to the pilot was the pitch attitude difference ($\Delta\theta$).

Two experienced pilot subjects (A and B) participated in the experiment. Pilot A is a current fixed-wing commercial airline pilot, a former Royal Navy rotary-wing pilot and is a graduate of the Empire Test Pilot School. Pilot B is a current military rotary-wing test pilot.

Experimental Results

The simulation results are summarized in Figure 39 and Figure 40. In these figures, the cutoff frequency (ω_{cut}) is adopted to measure the frequency of pilot control activity applied [36].
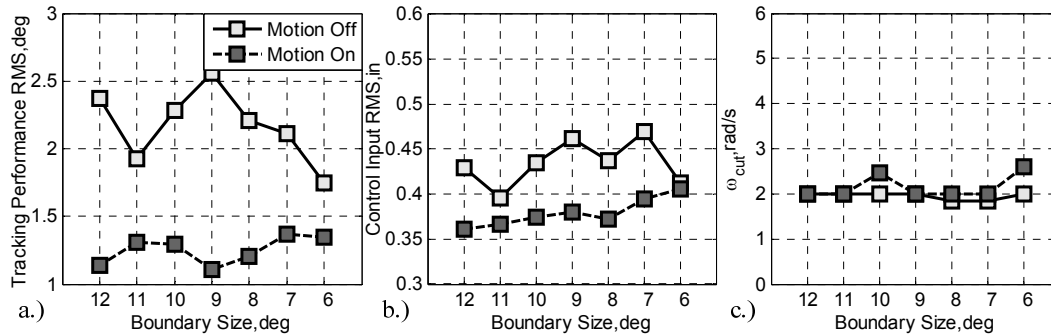
Figure 39 Illustration of tracking performance and control activities for Pilot A
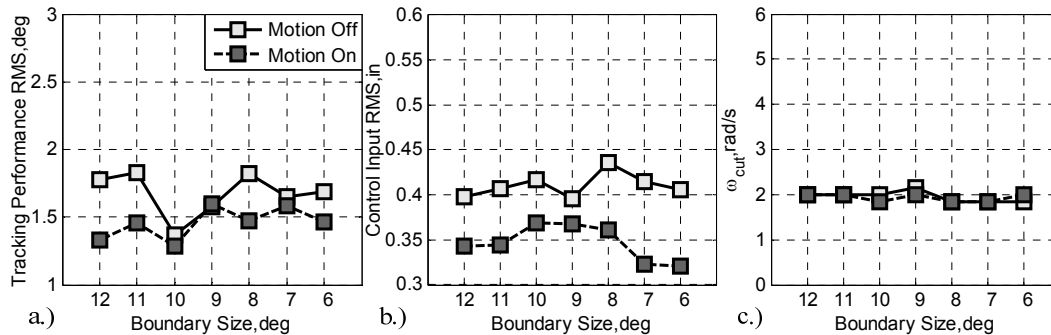

Figure 40 Illustration of tracking performance and control activities for Pilot B

Figure 39 and Figure 40 can be used to compare the results of the simulation experiment with the predictions made earlier in the Section. In accordance with those predictions, Figure 39a and Figure 40a show a different tracking performance between the motion-on and –off cases for both pilots. In general, the observed motion-off tracking performance is worse (larger RMS values) than the motion-on tracking performance. These findings are consistent with the theoretical analysis of section 4.1.2 whereby the inclusion of the vestibular and proprioceptive feedback loops/cues reduces the effective time delay in the pilot-vehicle system, thus increasing the closed-loop performance.

Figure 39b and Figure 40b, in agreement with the predicted behaviour trend, show different control activity (in terms of different control input sizes) from both pilots. Figure 25 can be used to help explain these observations. First, using the methodology based on optical τ information [41], the average τ_{min} values were found to be: -1.4 s (Pilot A) and -1.2 (Pilot B) for motion off, and -1.1 s (Pilot A) and -1.1 (Pilot B) for motion off. These τ_{min} values, as well as the degraded (generally) tracking performance as boundary size decreases (motion on), indicates that the

related (τ_{min}, K_b) pairs are located within the inner-left (darker shaded) regions of Figure 25. Meanwhile, for motion on, the small control input variation shown in Figure 39b and Figure 40b indicates only a small variation in K_b values. Combined with the wider bandwidth in Figure 22 and the larger stable region in Figure 24, this would lead to the observed small variation in control input with motion on, and similarly the larger variation with motion off.

Although the trends indicated above are consistent with the model predictions, it should be noted that the experimental tracking RMS values achieved (1.3 – 2.5 deg) are nearly twice as large as the related theoretical ones (< 1 deg) based upon their posited location in Figure 25. The differences can mainly be accounted for as follows. First, there is a time delay in the HELIFLIGHT-R simulator due to filters, actuator dynamics, and digital system delays that contribute an incremental time delay of approximately 125 ms between inceptor input and cue initiation. This time delay value was not included in the original theoretical analysis (Figure 19 and Figure 20) but it can have a significant influence on the closed-loop performance, such as reducing ω_c and deteriorating the tracking performance. The former effect is evident in Figure 41 (for

motion off), where the analysis has been re-run with a time delay of 200 ms. By comparing this figure with Figure 22, it is apparent, particularly at low τ_{min} and K_b values, that there is the expected reduction in system bandwidth.
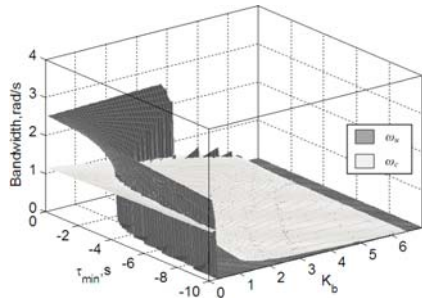

Figure 41 Bandwidth variation with time delay (200 ms, motion off)

Figure 42 shows the effect on the analysis that resulted in Figure 25 with the time delay included. It is now evident that the predicted error is more consistent with that observed in the experiment (again, in the left-hand darker shaded region), albeit at the upper end of the observations.
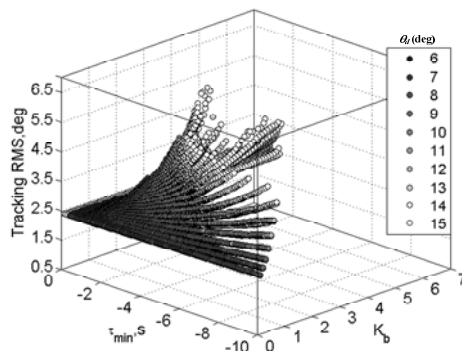

Figure 42 Tracking RMS variation with different K_b and τ_{min} values with time delay (200 ms, motion off)

It was also posited above that the tracking performance of a pilot was likely to be more variable with motion-off and more consistent with motion-on. Figure 39a and Figure 40a arguably show that this to be the case, particularly for Pilot A. For the motion-on cases for both pilots, there is an apparent steady trend for a generally worse target tracking performance as the boundary size decreases, but with a variation of much less than 0.5 deg. For pilot A, with motion off, the trend is generally for increased tracking performance with decreasing boundary size but with a variation of around 1 deg. For pilot B, the trend is arguably neutral with a variation of between 0.5 and 0.75 deg. these results also support the, perhaps unhelpful hypothesis, that tracking performance can both increase and decrease with decreasing boundary size.

Figure 39c and Figure 40c have been included to verify the pilot cut-off frequency assumption in the implemented multi-loop PT pilot model. It can be seen that the cutoff frequency values (ω_{cut}) of both pilots obtained from the experiments generally approach the desired 2 rad/s used to build the PT pilot model. This indicates that the two pilots tended to adopt a similar control bandwidth, but with a different control effort shown, in Figure 39b and Figure 40b, despite the imposed boundary.

The final prediction made using the model was that BAT PIOs would be difficult to trigger but that it would be easier to do so with motion cueing off. This was based upon the fact that to be able to generate a simulated BAT PIO, K_b has had to be increased up to be an "excessive" value (6) and when this was done, ω_u reached a high value of 8 rad/s. It has also been found to be difficult to trigger a BAT PIO experimentally without further reducing the workload margin, defined as the pilot's capacity to accomplish additional tasks [37]. Indeed, for the experimental campaign conducted for this paper, it was also found to be very difficult to trigger a BAT PIO event. In the end, to address this difficulty, a 100 ms transport delay, which is equivalent to increasing the pilot's lead control effort in the PT pilot model, had to be introduced to trigger a BAT PIO. The only BAT-PIO case available from this experiment is illustrated in Figure 43. It should be noted, that, in line with the predictions, this could only be achieved with the simulator motion cues turned off.
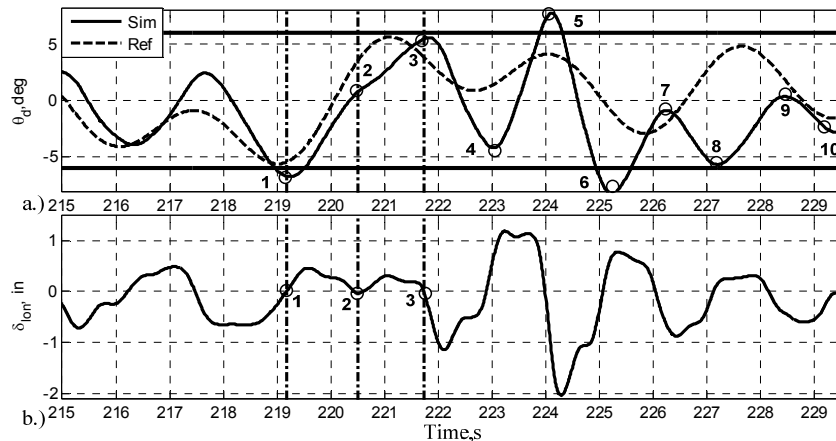
Figure 43 Illustration a BAT PIO with additional 100 ms transport time delay (Pilot A, motion-off)

The short-duration large amplitude oscillatory sequence in Figure 43 has a frequency of 2.7 rad/s. This is close to the theoretically predicted maximum ω_u value of 2.5 rad/s in Figure 41. Following this event, Pilot A also commented, unprompted, that at or around Point 2 in the manoeuvre, he became aware of the impending upper boundary. At this point, he had to divert part of his attention from the original full PT task to deal with this new situation. This apparent reference to a split between attention on the PT and BAT tasks lends further support the BAT pilot model structure proposed in Figure 8.

Categorization of the BAT PIO

As previously stated, a BAT PIO results from the situation when a pilot tries to avoid a boundary or a limit that may cause damage or death [21]. This phenomenon appears to be similar to the C-PIO, such as the oscillatory characteristics and large control inputs shown in Figure 43. Therefore, a question naturally arises as to the position of the BAT PIO within the following classical Cat I, Cat II, Cat III PIO. The remaining section of the paper is devoted to a brief discussion as to where BAT PIOs fit within this scheme.

Based on the results found in this paper thus far, the following specific features of the BAT PIO can be summarized. First, the BAT PIO is pertinent to a high-workload operation. As described above, the BAT pilot model in Figure 8 consists of a PT component that is for the primary control task and a BA component that is responsible for the "unexpected" task, modelled as a parallel processing operation. The appearance of this "unexpected" BA task can place a heavy load on the attentional demands of the pilot for both tasks and consequently, the workload margin for other operations (e.g., observing the instrument panel) is substantially reduced. The major consequences of the reduction in workload margin are reflected by a significant increase in control activity and degraded closed-loop task performance, shown in Figure 27, or the BAT-PIO case in Figure 43.

Second, the BAT PIO represents a transition situation in pilot behavioural organization i.e. a switching (or at least, a partial switching) of a key control variable. The BA process can actually be described as the compensatory control activity to maintain a safe distance to the impending boundary for a certain period. Therefore, during the BAT period, the pilot control behaviour (Figure 8 and in Figure 43) actually switches from being full-attention primary pursuit to being compensatory in nature. This pursuit-to-compensatory description for the BAT process not only complies fully with the original definition of this transition given by McRuer [12] but with the two examples he gave there. The first example describes that, to avoid a crash with an on-coming truck, the driver abandons a pursuit operation associated with a stare mode with a far-ahead fixation point and shifts to closer-in perception of truck-car clearance. The second example relates to a pilot tracking the deck for a carrier approach. Besides the consistent description between McRuer's pursuit-to-compensatory transition pilot behaviour and Gray's BAT pilot model, the findings from both this paper and McRuer's theoretical analysis on these examples show the same kind of system bandwidth (ω_c) and dynamic performance reduction. These performance degradations have been considered as one of the major PIO triggers [13] and lead to the BAT PIO, as found in this paper (in Figure 43).

Therefore, the BAT PIO is a high-workload phenomenon involving pilot dynamic transition. This property follows the following definition for Category III PIO as follows [21],"*Category III-Essentially Non-Linear Pilot-Vehicle System oscillations with Transition: These PIOs fundamentally depend on nonlinear transitions in either the effective controlled element dynamics, or in the pilot's dynamics.*

……Pilot transitions may be shifts in dynamic behavioural properties (e.g., from compensatory to synchronous), from modifications in cues (e.g., from attitude to load factor), or from behavioural adjustments to accommodate task modifications." Therefore, with regards to the last sentence of the Category-III PIO definition and the above discussion, it is proposed that the BAT PIO be considered to be a Category III PIO.

5. CONCLUSIONS

The goal of the present paper was to give an overview of the work performed in the ARISTOTEL project on rotorcraft rigid body RPC. Rigid body RPC involve adverse coupling phenomena dominated by helicopter lower frequency dynamics with pilot in the loop. Using as example the Bo-105 helicopter enhanced by a rate command attitude hold control system, the paper demonstrated that:

- The bandwidth criterion can be applied for Cat I PIO prediction, its effectiveness depending on the manoeuvres performed in the simulators. In fact, the results depend very much on how well the manoeuvre was designed to unmask the RPC

- The OLOP criterion for Cat II PIO prediction is dependent on the pilot gain , in the pitch axis, a good pilot rating trend existing with all rate limits used

The paper presented novel pilot modelling tools and novel prediction and detection RPC criteria. First, a new real time PIO detection tool was presented, the so-called Phase aggression Criterion (PAC) which was later developed into a prediction algorithm (PRE-PAC). The paper exemplified how to use PRE-PAC in order to either assess traditional RPC metrics or to 'map' the RPC incipience against pilot signal. Next, the boundary avoidance tracking (BAT) concept was discussed showing how it can be used to unmask Cat III PIO. Finally, bifurcation analysis was applied to pitch and roll tracking tasks. It was showed that, in the pitch axis, the performance of the bifurcation analysis is comparable to OLOP criterion. Concluding, it is believed that the novel tools developed in the ARISTOTEL project will contribute to unmasking the rigid body RPCs in future designs.

Acknowledgements

REFERENCES

1. McRuer, D.T., PIO- a historical Perspective, AGARD AR-335, Flight Vehicle Integration Panel Workshop on Pilot Induced Oscillations, Feb 1995

2. Pavel, MD. Et. Al., Present and Future Trends in Rotorcraft Pilot Couplings (RPCs) – A Retrospective Survey of Recent Research Activities within the European Project ARISTOTEL, 36th European Rotorcraft Forum, Gallarate, Italy, 13-14 September 2011

3. Pavel MD et. Al., A Retrospective Survey of Adverse Rotorcraft Pilot Couplings in European Perspective, AHS 68th Annual Forum and Technology Display, Fort Worth, Texas, USA, 1-3 May 2012

4. McRuer, D.T., et al., "AVIATION SAFETY AND PILOT CONTROL. Understanding and Preventing Unfavorable Pilot-Vehicle Interactions", *ASEB National Research Council*, National Academy Press, Washington D.C., 1997

5. Gibson, J.C., Development of a Methodology for Excellence in Handling Qualities design for fly by wire aircraft", Delft University Press, ISBN 90-407-1841-5, 1999

6. Curtiss, H. C, "Stability and Control Modelling," Vertica, Vol 12 (4), 1988, pp. 381-394

7. Heffley, R. K., Bourne, S., Curtiss, H. C , Hindson, W S., and Hess, R. A., "Study of Helicopter Roll Control Effectiveness," NASA Contractor Report, 177404, 1986

8. Dryfoos, J. B., and Kothmann, B. D., "An Approach to Reducing Rotor-Body Coupled Roll Oscillations on the RAH-66 Comanche Using Modified Roll Rate Feedback," American Helicopter Society 55th Annual National Forum Proceedings, Montreal, Canada, May 1999, pp. 1127-1140

9. McRuer, Duane, Human Dynamics and Pilot Induced Oscillations, Minta Martin Lecture, Dec. 1992, MIT, Massachusetts

10. Padfield, GD, Dequin, A., Haddon, David, Kampa, K., Basset, P., Grunhagen, W.von, Haverdings, H., McCallum, A.T. Predicting Rotorcraft Flying Qualities Through Simulation Modelling; A Review of Key Results From GARTEUR AG06, DERA, U.K, 2006

11. Tischler, M.B., Digital Control of Highly Augmented Combat Rotorcraft, NASA TM-88346, May 1987

12. McRuer, D.T., "Pilot-Induced Oscillations and Human Dynamic Behaviour", NASA CR-4683, 1995

13. McRuer, D.T., an Krendel, E.S., Mathematical Models of Human pilot behaviour, AGARD AG-118, Jan 1974

14. Duda, H., Prediction of Pilot in the loop oscillations due to rate saturation, J. of Guidance, Control and Dynamics, Vol 20, no3, May-June 1997, pp. 581-587

15. McRuer, D.T., Krendel, E.S., The human operator as a servo system element, J. Franklin Institute vol. 267, no 5, pp381, May 1959 and No6. P.511, June 1959

16. Elkind, J.I., A survey of the development of models for the human controller, in R.C. Langford, CJ Mundo Eds., Guidance and Control II, vol 13 of Progress in Astronautics and Aeronautics, Academic Press, New York, 1964

17. McRuer D.T., Jex, H.R., A review of Quasi-Linear Pilot models, IEEE trans vol HFE-8, no.3, pp.231-249, 1967

18. Mariano, Valeria, Guglieri, G., Ragazzi, A., Application of pilot induced oscillations prediction to rotorcraft, 37th European Rotorcraft Forum, Gallarate, Sept. 13-15, 2011

19. Pavel, M.D. et. Al., Adverse rotorcraft pilot couplings – Past, present and future challenges, Progress in Aeronautical Sciences, 2013

20. Yilmaz, D., Pavel. MD, Jones, M., Jump M., Lu, L,. Identification of Pilot Control Behavior during Possible Rotorcraft Pilot Coupling Events, 38th European Rotorcraft Forum, Amsterdam, the Netherlands, September 4 – 7, 2012

21. Gray III, W. R., "Boundary-Avoidance Tracking: A New Pilot Tracking Model," AIAA Atmospheric Flight Mechanics Conference and Exhibit, San Francisco, California, Aug., 2005, pp. 86-97

22. Lee, D. N., "Guiding Movement by Coupling Taus," *Ecological Psychology*, published online 1998; Vol. 10, No. 3, pp. 221-250

23. Gibson, J. J., "The Perception of the Visual World," *American Journal of Psychology*, Vol. 64, 1951, pp. 622-625

24. Jones, M., Jump, M., Lu, L., Pavel, M., and Yilmaz, D., "The Use of the Phase-Aggression Criterion for Identification of Rotorcraft Pilot Coupling Events," *38th European Rotorcraft Forum*, Amsterdam, Netherlands, Sept. 4th-7th 2012

25. Hess, R.A., "Simplified Approach for Modelling Pilot Pursuit Control Behaviour in Multi-Loop Flight Control Tasks," *Proceedings of the I MECH E Part G Journal of Aerospace Engineering*, published online 2006; Vol. 220, No. 2, pp. 85-102

26. Hess, R.A., "Obtaining Multi-Loop Pursuit-Control Pilot Models From Computer Simulation," *Proceedings of the I MECH E Part G Journal of Aerospace Engineering*, published online Feb. 2008; Vol. 222, No. 2, pp. 189-199

27. Hess, R.A., and Siwakosit, W., "Assessment of Flight Simulator Fidelity in Multiaxis Tasks Including Visual Cue Quality," *Journal of Aircraft*, published online Jul. 2007; Vol. 38, No. 4, pp. 607-614

28. Hess, R. A., and Marchesi, F., "Analytical Assessment of Flight Simulator Fidelity Using Pilot Models," *Journal of Guidance, Control, and Dynamics*, published online May. 2009; Vol. 32, No. 3, pp. 760-770

29. Gray III, W. R., "Handling Qualities Evaluation at the USAF Test Pilot School," Proceedings of the AIAA Atmospheric Flight Mechanics Conference 10 - 13 August 2009, Chicago, Illinois

30. Warren, R. D., "An Investigation of the Effects of Boundary Avoidance on Pilot Tracking," Air Force Inst. of Tech., Wright-Patterson AFB, OH. Graduate School of Engineering and Management, Dec., 2006

31. McRuer, D. T., Clement, W. F., Thompson, and R. E. Magdaleno, "Minimum Flying Qualities Volume II: Pilot Modelling For Flying Qualities Application," Flight Dynamics Laboratory, Air Force Systems Command, Wright-Patterson Air force Base, OHIO,WRDC-TR-89-3125, Jan.1990

32. Jump, M., Hodge, S., Dang Vu, B., Masarati, P., Quaranta, G., Mattaboni, M., Pavel, M. D., and Dieterich, O., "Adverse Rotorcraft-Pilot Coupling: Test Campaign Development at the University of Liverpool," *34th European Rotorcraft Forum*, Liverpool, England, Sept. 16th -18th 2008

33. Blake, R.D. *Boundary Avoidance Tracking: Consequences (and Uses) of Imposed Boundaries on Pilot-Aircraft Performance*, MSc Thesis, Department of the Air Force, United States Air Force Institute of Technology, Wright-Patterson Air Force Base, Ohio, 2009

34. Dotter, J. D., "An Analysis of Aircraft Handling Quality Data Obtained From Boundary Avoidance Tracking Flight Test Techniques," Air Force Inst. of Tech., Wright-Patterson AFB, OH. Graduate School of Engineering and Management, Mar., 2007

35. White, M. D., Perfect, P., Padfield, G. D., Gubbels, A. W., and Berrayman, A. C., "Acceptance Testing of A Rotorcraft Flight Simulator for Research and Teaching: the Importance of Unified Metrics," *35th European Rotorcraft Forum*, Hamburg, Germany, Sept. 22th - 25th 2009

36. Lampton., A., and Klyde, D. H., "Power Frequency: A Metric for Analyzing. Pilot-in-the-Loop Flying Tasks," *Journal of Guidance, Control, and Dynamics*, published online Sept. 2012; Vol. 35, No. 5, pp. 1526-1537. doi: 10.2514/1.55549

37. Allen, R. W., Clement, W. F., and Jex, H. R., "Research on Display Scanning, Sampling, and Reconstruction Using Separate Main and Secondary Tracking Tasks," NASA Contractor Report CR-1569, NASA Contractor Report CR-1569, Jul. 1970

38. Anon. Aeronautical Design Standard ADS33E-PRF, Performance Specification, Handling Qualities Requirements for Military Rotorcraft. US

Army AMCOM, Redstone, Alabama, March 21, 2000

39. Mitchell, D.G., PIO Detection with a Real-time Oscillation Verifier (ROVER), Viewgraphs presented at NASA Dryden Flight Research Center, April 8th, 1999. NASA/CP-2001-210389/Vol.2

40. Suliman, S. ,Yilmaz, D. and Pavel, M. Harmonizing the Realtime Oscillation Verifier (ROVER) with Handling Qualities Assessment for Enhanced Rotorcraft Pilot Couplings Detection, Proceedings of the 38th European Rotorcraft Forum, Amsterdam, Netherlands, 2012

41. Jones M., ,Jump M, Lu L. A new method for near real-time rotorcraft pilot coupling detection and identification. Journal of Guidance, Control and Dynamics 2012;35(1):80–92.

42. Dieterich, O., Götz, J., Dang-Vu, B., Haverdings, H., Masarati, P., Pavel, M., Jump, M. and Gennaretti, M., Adverse Rotorcraft-Pilot Coupling: Recent Research Activities in Europe, 34th European Rotorcraft Forum, Liverpool, UK, 2008

43. Jump, M., and Padfield, G.D., Investigation of the Flare Manoeuvre Using Optical Tau, J Guid Contr Dynam, Sept.2006, 29, (5), pp. 1189-1200

44. Ioos, G. and Joseph, D.D., Elementary Stability and Bifurcation Theory. Springer Verlag, 1981

45. Marsden, J.E. and Mc Cracken, M., The Hopf Bifurcation and its Applications. Springer Verlag, 1976

46. GARTEUR FM AG-12, Analysis of Non-Linear Pilot-Vehicle Systems Using Modern Control Theory, TP-120-02, 2000

47. Mehra, R.K., Prasanth, R.K., Bifurcation and Limit Cycle Analysis of Non-linear Pilot, AIAA Paper 98-4249, 1998

48. Halanay, A., Ionita, A., Safta, C.A., Hopf Bifurcations through Delay in Pilot Reaction in a Longitudinal Flight, Nonlinear Dyn, No 60, pp 413–423, 2010

49. GARTEUR FM AG-12, PIO Analysis of a Highly Augmented Aircraft, TP-120-07, 2001